

# Geology of the Kinskuch Lake area and Big Bulk porphyry prospect: Syndepositional faulting and local basin formation during the Rhaetian (latest Triassic) transition from the Stuhini to the Hazelton Group



E.A. Miller<sup>1, a</sup>, L.A. Kennedy<sup>1</sup>, and B.I. van Straaten<sup>2</sup>

<sup>1</sup> Department of Earth, Ocean and Atmospheric Sciences, The University of British Columbia, Vancouver, BC, V6T 1Z4

<sup>2</sup> British Columbia Geological Survey, Ministry of Energy, Mines and Petroleum Resources, Victoria, BC, V8W 9N3

<sup>a</sup> corresponding author: emiller@eoas.ubc.ca

Recommended citation: Miller, E.A., Kennedy, L.A., and van Straaten, B.I., 2020. Geology of the Kinskuch Lake area and Big Bulk porphyry prospect, northwestern British Columbia: Syndepositional faulting and basin formation during the Rhaetian (latest Triassic) transition from the Stuhini to the Hazelton Group. In: Geological Fieldwork 2019, British Columbia Ministry of Energy, Mines and Petroleum Resources, British Columbia Geological Survey Paper 2020-01, pp. 77-99.

## Abstract

The Stewart-Iskut district, in the Stikine terrane of northwestern British Columbia, contains numerous Late Triassic to Early Jurassic porphyry Cu-Au and epithermal deposits. These deposits are broadly coeval with the transition from volcano-sedimentary deposits of the Stuhini Group (Late Triassic) to those of the Hazelton Group (latest Triassic to Jurassic), which is marked by strata bearing evidence of significant uplift and erosion. Recent studies in the district have proposed that small pull-apart basins served to localize emplacement of the KSM Cu-Au porphyry system. Detailed (1:10,000 scale) mapping in the Kinskuch Lake area near the Big Bulk Cu-Au porphyry prospect, 50 km southeast of Stewart, indicates that syndepositional faulting in the Rhaetian (latest Triassic) strongly influenced the transition from Stuhini Group to Hazelton Group deposition. Conglomerates, informally referred to herein as the Kinskuch conglomerates, containing Stuhini Group-derived megaclasts (up to 120 m) at the base of the Hazelton Group signify a high-relief, fault-generated paleotopography and mark a fundamental break in the tectonic history of the region. Progressive stripping into deeper parts of the subjacent Stuhini Group section, as recorded by bottom-to-top clast compositions that yield an inverse stratigraphy, signify at least 400 m of Stuhini Group unroofing. These conglomerates are limited to the east side of a prominent northeast-trending dextral fault (Tabletop fault). We propose that the Tabletop fault and likely other northeast-trending faults in the area had an earlier (latest Triassic) history with strike-slip or oblique movement, and that releasing step-overs, splays, or double bends in this fault network created local zones of north-south extension, easterly trending normal faults, and local pull-apart basins. The Big Bulk porphyry diorite stock (204.61 ± 0.18 Ma, CA-TIMS, U-Pb zircon, this study), which cuts the lower part of the Hazelton Group, has four intrusive phases all of which are approximately tabular with an east-west trend. Main stage Cu-Au mineralization is in sheeted quartz-chalcopyrite veins, with easterly orientations, consistent with local northerly extension during porphyry emplacement. Hence, like other areas in northwestern Stikinia, sedimentation, magmatism, and porphyry mineralization appear to have had a strong structural control. Along with the prominent northeast-trending strike-slip faults, mid-Cretaceous shortening related to the Skeena fold and thrust belt is expressed as southeast- and east-vergent thrusts and folds. It is likely that many of the mid-Cretaceous structures in the area reactivated pre-existing structures.

**Keywords:** Kinskuch conglomerates, Big Bulk, Stewart-Iskut district, Hazelton Group, Stuhini Group, Rhaetian, Late Triassic, Early Jurassic, syndepositional faulting, Triassic-Jurassic porphyry, Cu-Au porphyry

## 1. Introduction

The Kinskuch Lake area is in the Stikine terrane (Stikinia) of the Canadian Cordillera (Fig. 1), near the southern end of the Stewart-Iskut district, a >200 km-long belt of porphyry Cu-Au and epithermal Au mineralization that is hosted by Upper Triassic rocks of the Stuhini Group and overlying uppermost Triassic to Lower Jurassic rocks of the Hazelton Group (Fig. 2a). The Stewart-Iskut district extends from Kitsault northward to Stewart and the Stikine River, in the southern part of a region popularly referred to as the ‘Golden Triangle’.

Many mineral deposits in the Stewart-Iskut district are on or near north-south and east-west trending faults and lineaments.

Many faults were likely long lived, and such pre-existing structures were probably important in localizing mineralization (Nelson and Kyba, 2014; Kyba and Nelson, 2015; Febbo et al., 2019). These fault systems may have originated in the Paleozoic basement of Stikinia. Some were reactivated in the Cretaceous (Nelson and Kyba, 2014; Febbo et al., 2019), some in the Eocene (Tombe et al., 2018), and others had a controlling influence on rocks as young as those at the Mount Edziza volcanic complex (Miocene-Holocene; Edwards and Russell, 2000; Febbo et al., 2019).

Although porphyry Cu-Au-Mo systems, especially those formed along active continental margins, form in overall

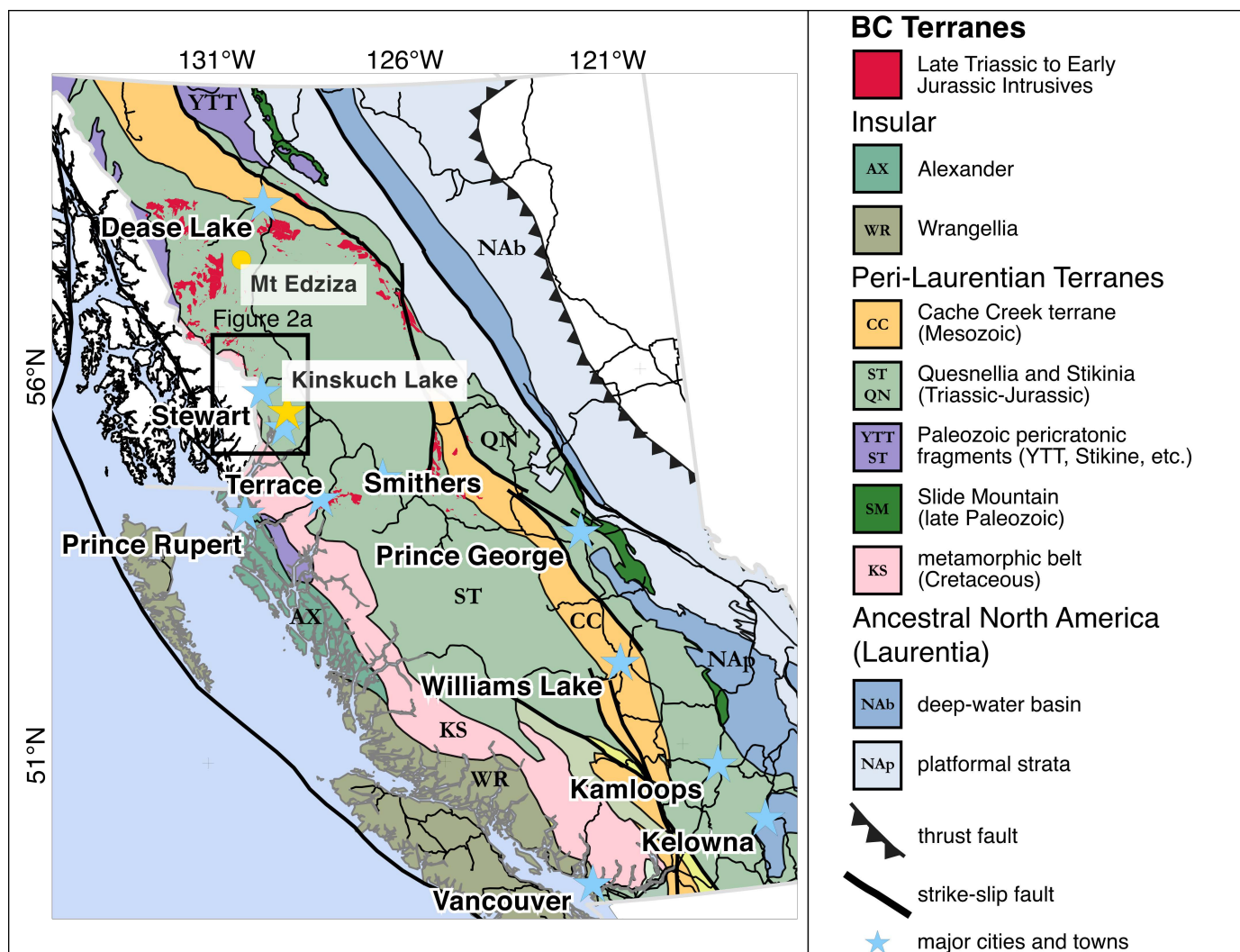


Fig. 1. Location of the Kinskuch Lake area with respect to terranes of British Columbia (after Colpron and Nelson, 2011).

contractional tectonic environments (Tosdal et al., 2009; Sillitoe, 2010), some form in local zones of extension or in zones of pre-existing extensional crustal architectures (e.g., Richards et al., 2001; Richards, 2003; Gow and Walshe, 2005; Cloos and Sapiie, 2013; Piquer et al., 2015). Studies by Nelson and Kyba (2014) and Febbo et al. (2019) at the Kerr-Sulphurets-Mitchell (KSM) deposit demonstrate that syndepositional faulting and coarse siliciclastic deposition accompanied Early Jurassic porphyry emplacement. They proposed that small pull-apart basins along reactivated basement structures served to localize emplacement of individual intrusions of the KSM porphyry system.

To test this model regionally and to better understand the uppermost Triassic to Lower Jurassic structural and tectonic setting of the Stewart-Iskut belt, we undertook detailed (1:10,000 scale) mapping in the Kinskuch Lake area near the Big Bulk porphyry prospect (Fig. 2b), which has characteristics and stratigraphy similar to the KSM deposits. Herein, we present lithological descriptions, stratigraphic analysis, structural data,

and geochronology to infer the depositional and structural setting at Kinskuch Lake before and during emplacement of the Big Bulk porphyry system. Our observations at Kinskuch Lake show that syndepositional faulting strongly influenced the transition from the Stuhini Group to the Hazelton Group during the latest Triassic.

**2. Regional geology and tectonic setting**

The Stikine volcanic island arc terrane encompasses three unconformity-bounded arc-related volcano-sedimentary successions: the Stikine assemblage (Paleozoic); the Stuhini Group (Upper Triassic); and the Hazelton Group (uppermost Triassic to Middle Jurassic; Logan et al., 2000; Nelson et al., 2018). More than 90% of the known copper resources in British Columbia accumulated between ca. 211 and 199 Ma, spanning the transition from Stuhini Group arc development to Hazelton Group volcanism and sedimentation (Logan and Mihalynuk, 2014). Our study focusses on this transition.

Regionally, the Stuhini Group (Late Triassic) comprises

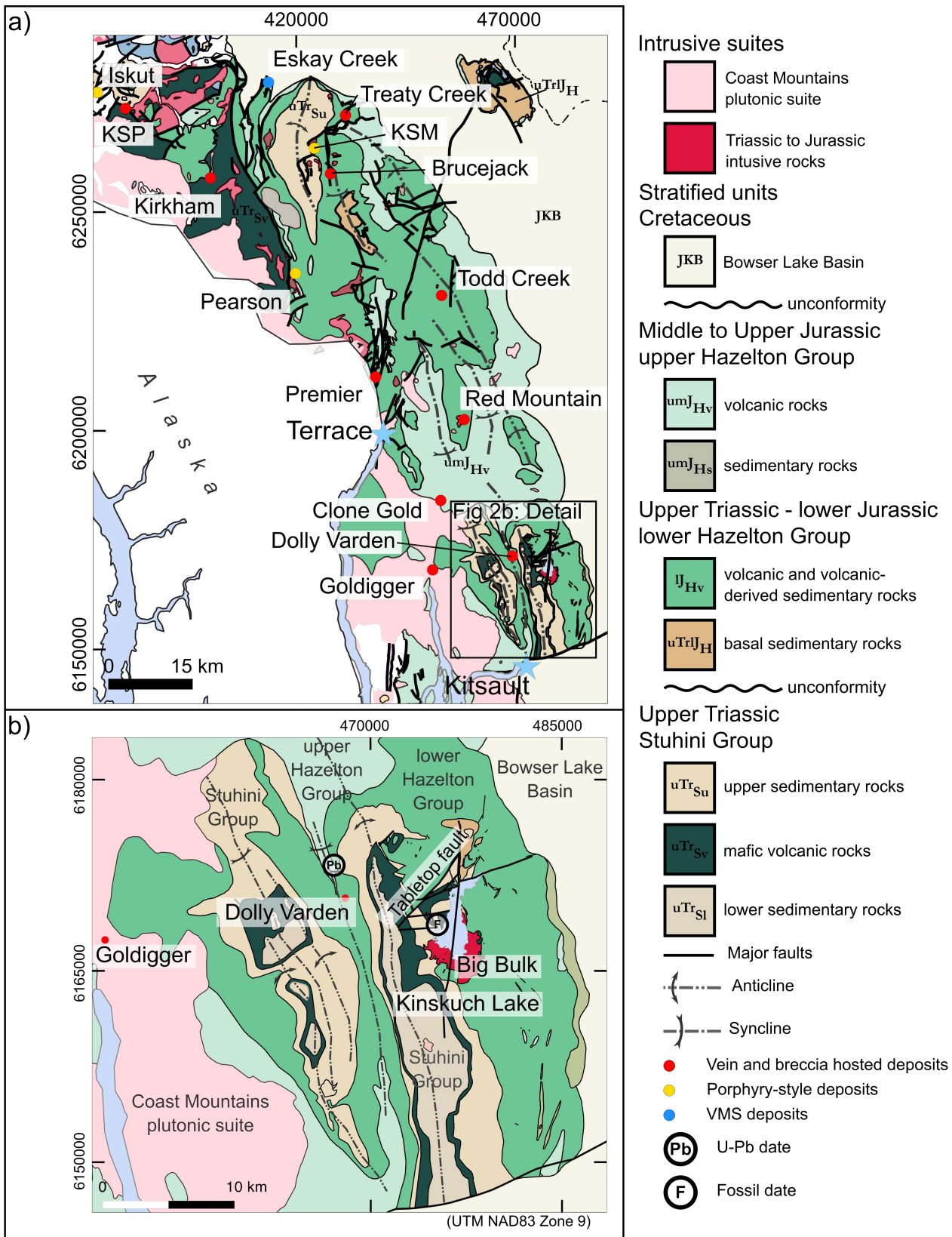


**Fig. 2. a)** Regional geological and structural setting (after Alldrick et al., 1986; Greig, 1992; and Colpron and Nelson, 2011), with selected Cu(±Au±Mo) porphyry (yellow) and vein and breccia-hosted (including epithermal) deposits (red). **b)** Local geological and structural setting (after Alldrick et al., 1986) with locations of geochronological samples: (Pb) 178.1 ± 2.2 Ma felsic tuff in the upper part of the Hazelton Group (U-Pb zircon, Hunter and van Straaten, 2020) and (F)-Rhaetian (latest Triassic) conodont sample (Cordey et al., 1992; Greig et al., 1995; and Golding et al., 2017).

augite-phyric mafic volcanic rocks, volcanic-derived sedimentary rocks, and marine sedimentary rocks including argillite, sandstone, minor limestone, and rare chert. The Stuhini Group is unconformably overlain by intermediate volcanic and volcanic-derived sedimentary rocks of the Hazelton Group (Nelson et al., 2013; 2018). Basal lower Hazelton Group rocks range from as old as latest Triassic (Rhaetian) to Early Jurassic (Hettangian-Sinemurian; e.g., Thorkelson et al., 1995; Barresi et al., 2015; Nelson et al., 2018; Hunter and van Straaten, 2020).

The lower part of the Hazelton Group (uppermost Triassic-Lower Jurassic) consists primarily of feldspar-hornblende-phyric volcanic rocks and volcanic-derived sedimentary rocks. Quartz-bearing sandstones and granitoid clast-bearing conglomerates of the Jack Formation at the base of the Hazelton Group near the KSM deposits and the lower Iskut River display evidence of syndepositional faulting (Nelson and Kyba, 2014). The upper part of the Hazelton Group (Early to Middle Jurassic) is predominantly a post-arc sedimentary package with local bimodal rift-related volcanic rocks (Iskut River Formation; Gagnon et al., 2012; Nelson et al., 2018). Although sections containing bimodal volcanic rocks have not been recognized in the Kinskuch Lake area, Hunter and van Straaten (2020) reported a U-Pb zircon age of  $178.1 \pm 2.2$  Ma from a felsic tuff in the nearby Kitsault River valley (Fig. 2b), similar to ages from the Iskut River Formation (see Nelson et al., 2018).

Stratified rocks of northwestern Stikine terrane are cut by several intrusions including: 1) the Stikine and Galore plutonic suites (Late Triassic), which are coeval and comagmatic with the Stuhini Group (Nelson et al., 2018); 2) the Tatogga (latest Triassic) and Texas Creek plutonic suites (Early Jurassic), which are coeval and comagmatic with the lower part of the Hazelton Group (Nelson et al., 2018); and 3) the Hyder plutonic suite (Eocene), the youngest intrusions in and east of the Coast Plutonic complex (Alldrick, 1993).

Rocks in the region were deformed in the mid-Cretaceous during development of the Skeena fold-and-thrust belt, which formed in response to sinistral transpression (Evenchick, 2000; Evenchick et al., 2007). The fold-and-thrust belt affects most of the central Intermontane belt and accommodates a minimum of 44% northeasterly directed shortening (Evenchick et al., 2007). By the middle to Late Cretaceous, large-scale dextral faults initiated, signalling a change in relative plate motions from earlier, predominantly sinistral kinematics (Nelson et al., 2013). The Paleocene to Eocene saw dextral-transensional tectonics, during which many pre-existing orogen-parallel structures accumulated significant offset (Nelson et al., 2013).

### 3. Methods

The map area is in a north-south elongate, ridge-bounded depression centred on Kinskuch Lake (Fig. 3). Outcrop is excellent, and mapping was at a scale of 1:10,000, with key sections selected for more detailed work, such as at the Big Bulk porphyry prospect where we mapped at a scale of 1:5,000.

Because of their importance (see below), conglomerate and megaclast-bearing beds at the transition between the Stuhini and Hazelton groups were given special attention. At 40 sites we did clast composition counts and determined the dimensions of the 10 largest clasts. These counts were completed by identifying 50 clasts along 20 cm-wide strips in lines perpendicular to bedding.

## 4. Lithostratigraphy

The oldest rocks in the area are Stuhini Group (Upper Triassic) augite-phyric basalts and marine sedimentary strata, which are primarily exposed on the western side of Kinskuch Lake (Fig. 3). Hazelton Group rocks are mostly exposed on the eastern side of the lake. To ease the following discussion, we illustrate stratigraphic relationships within and between the Stuhini and Hazelton groups in a north-south transect (Fig. 4). The 'Big Bulk' porphyry is on the southeast and south sides of the lake. The area is cut by numerous small, likely Eocene, dikes.

### 4.1. Stuhini Group (Upper Triassic)

The Stuhini Group consists of augite-phyric volcanic rocks, and sedimentary rocks including conglomerates with augite-bearing clasts, sandstones, argillite, sandstone, minor limestone, and rare chert. The volcanic rocks are exposed near the western shore of the central part of the lake and to the west (Figs. 2b, 3). The overlying sedimentary rocks are in low-lying exposures on the west side of the lake and only locally at low elevations in drainages and along the shoreline east of the lake.

#### 4.1.1. Volcanic and volcanic-derived sedimentary rock unit

The lower part of the Stuhini Group is typified by augite-phyric volcanic rocks and well-stratified, monomictic mafic volcanic clast-bearing conglomerate to volcanic-derived sandstone interstratified with lesser mafic volcanic breccia (Fig. 5a). The unit typically forms 10-50 m thick beds in which conglomerates and sandstones overlie coherent augite-phyric volcanic flows and associated volcanic breccia (Fig. 5b). Conglomerates directly overlying the flows contain angular to subrounded clasts. The flows generally have sharp basal contacts and locally contain subrounded augite-phyric clasts incorporated from underlying sedimentary beds alongside more angular, likely juvenile clasts of similar composition. Near the top of the unit volcanic breccias and augite-phyric coherent rocks gradually become more prominent, although interbedded with increasingly fine-grained sedimentary units. We define the top of the unit as the uppermost level containing coherent mafic flows.

#### 4.1.2. Sedimentary rock unit

This unit consists of interstratified argillite, feldspathic sandstone, conglomerate, and siltstone. Quartz is absent in all rock types. We have divided the unit into two facies mappable at the 1:10,000 scale.



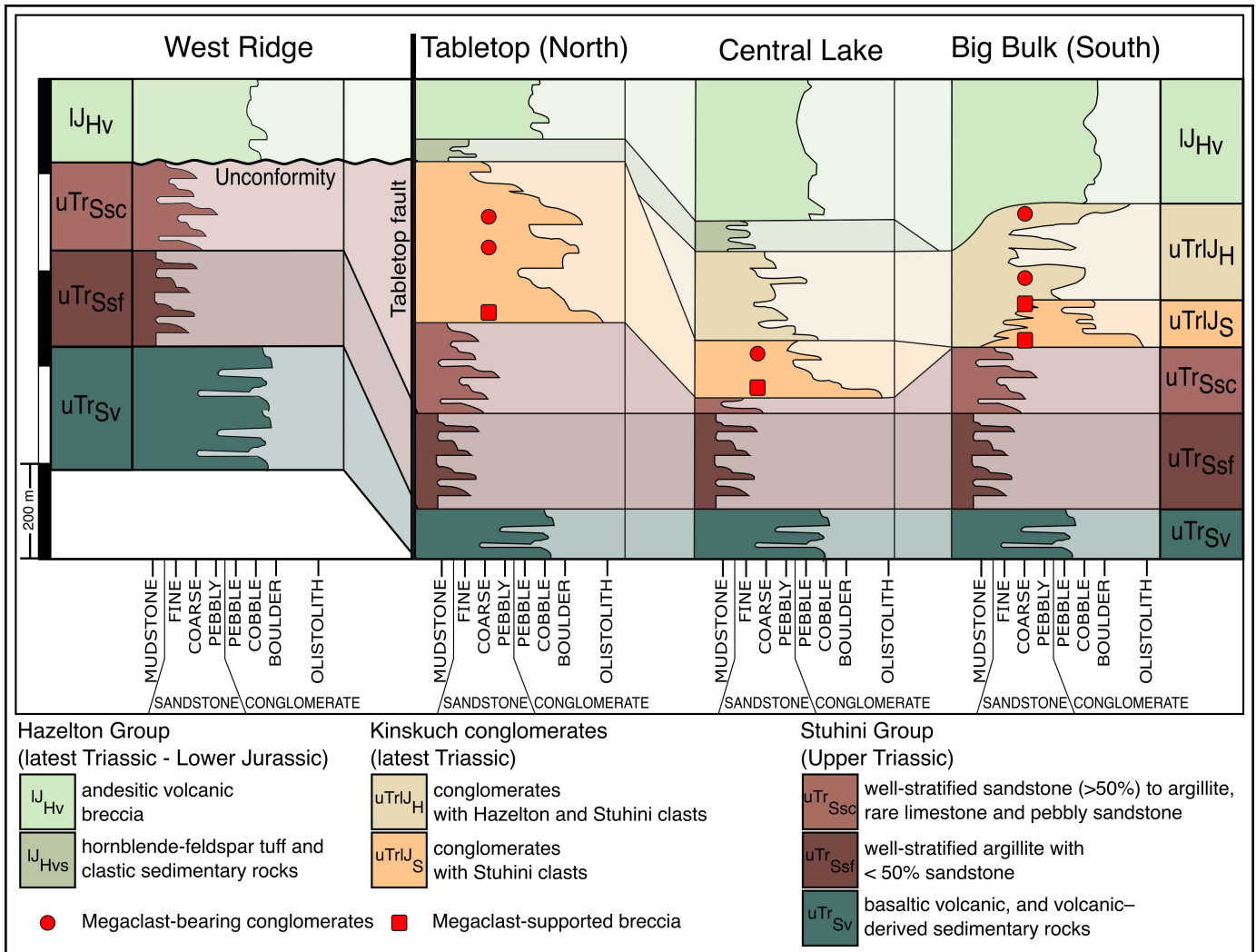


Fig. 4. Schematic north-south stratigraphic cross section illustrating lithologic variations in the Stuhini and Hazelton groups.

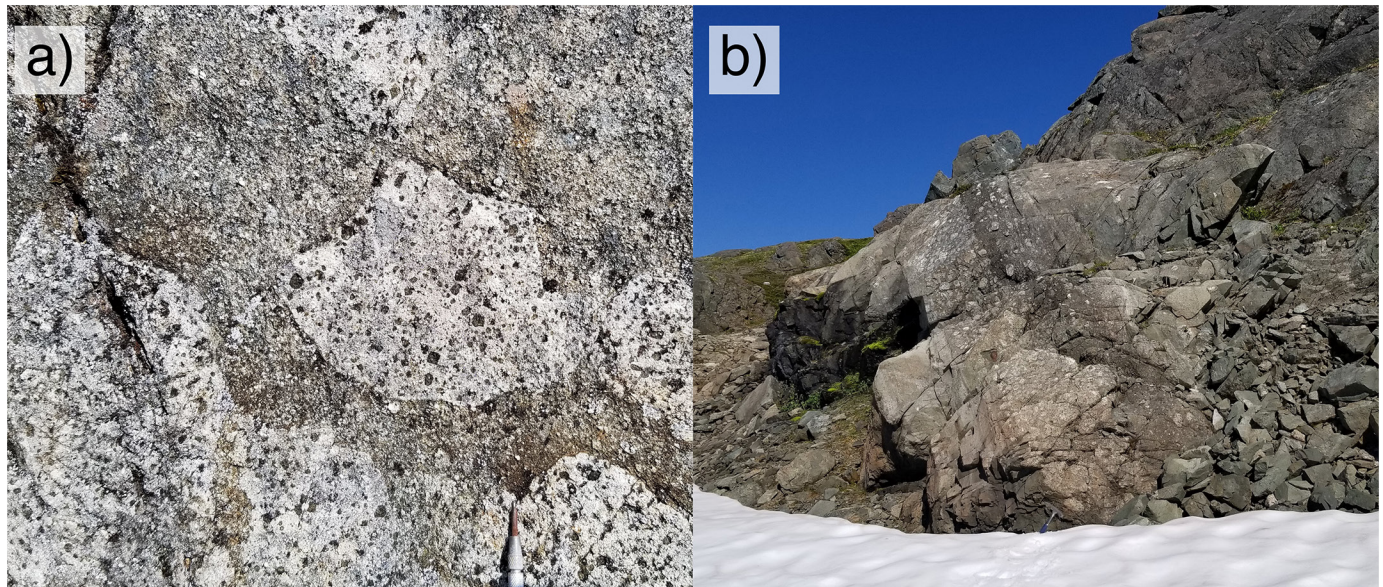


Fig. 5. Stuhini Group volcanic and volcanic-derived sedimentary rocks. **a)** Matrix-supported volcanic breccia with angular augite-phyric clasts and augite phyric groundmass (uTr<sub>Sv</sub>; 473840E, 6168792N). **b)** Volcanic breccia (base of outcrop at left of photo) and interstratified volcanic-derived conglomerates and sandstones younging upward to the north (uTr<sub>Sv</sub>; 472194E, 6172116N UTM NAD83 Zone 9; looking west).

#### 4.1.2.1. Fine-grained sedimentary facies

This facies consists of more than 50% well-bedded argillite and mudstone (locally graphitic), with 1 to 20 cm-thick interbeds of siltstone and very fine- to fine-grained sandstone and lesser, medium-grained sandstone. It also includes rare (<5%) coarse-grained sandstone and pebbly sandstone. Upsection, the number and thicknesses of sandstone beds increases and the proportion of mudrocks decreases as the facies passes gradationally to the compositionally similar coarse-grained sedimentary facies.

#### 4.1.2.2. Coarse-grained sedimentary facies

This facies consists of more than 50% well-bedded siltstone, lithic sandstone, feldspathic sandstone, and pebbly sandstone, with lesser argillite and mudstone (Fig. 6a), rare calcareous sandstone (Fig. 6b), and fossiliferous limestone (Fig. 6c) of limited lateral extent. It represents an upward coarsening from the underlying fine-grained sedimentary facies.

### 4.2. Hazelton Group

#### 4.2.1. Kinskuch conglomerates (latest Triassic; new name)

This new informal unit consists of massive to poorly stratified pebble to boulder conglomerate with rounded to angular clasts and local megaclasts (up to 120 m). The conglomerates are locally interstratified with lesser coarse-grained sandstone (ranging from lithic arkose to feldspathic litharenite) and pebbly sandstones, none of which contain quartz. Locally coarse-grained sandstone-filled channels cut conglomerates, commonly showing inverse graded bedding. Clast types include sandstone, mudstone, limestone, chert, and augite-phyric basalt similar to rocks in the Stuhini Group (Fig. 7) and hornblende-feldspar-phyric volcanic rocks similar to those in the Hazelton Group (Fig. 8). The conglomerates are generally clast supported with clasts set in a predominantly feldspathic matrix, with local carbonate sand grains and/or calcareous cement, to lesser muddy matrix. Neither the matrix nor the clasts appear to contain detrital quartz. The conglomerates contain rare muscovite and biotite-bearing clasts, including coarse biotite-bearing sandstone and muscovite schists in which internal fabrics are truncated at clast boundaries; the source of these clasts is unknown. The conglomerates are interstratified with basal Hazelton tuffs.

The Kinskuch conglomerates consistently overlie Stuhini Group sedimentary rocks southeast of the Tabletop fault and are absent northwest of the fault (Figs. 3, 4). On the eastern side of the lake they are observed at low elevations in some incised drainages below the steep, west-facing ridge of resistant Hazelton Group volcanic breccias. In northern and southern exposures, the conglomerates contain mainly cobble and larger fragments with minor pebbly interbeds. In contrast, most of the conglomerates in the ‘central lake’ exposures consist mainly of pebble conglomerates to pebbly sandstones with less abundant coarser beds (Fig. 9). Bedding in the conglomerates appears to be concordant with bedding in subjacent Stuhini Group. The transition from Stuhini Group rocks to Kinskuch conglomerates is typically marked by an abrupt change to boulder and



**Fig. 6.** Stuhini Group sedimentary rocks. **a)** Well-stratified, pale buff weathering feldspathic sandstone and dark-toned mudstone younging upright to the east from sharp-based fining-upward sequences and sandstone load cast and flame structures (uTrSsc) looking S. **b)** Rhythmically interlayered buff weathered feldspathic sandstone and black argillite with lesser recessive calcareous sandstone beds (uTrSsc) looking north, tops to west. **c)** Grey to buff-weathered fossiliferous limestone (uTrSsc). These limestones are found as clasts in the Kinskuch conglomerates (see below).

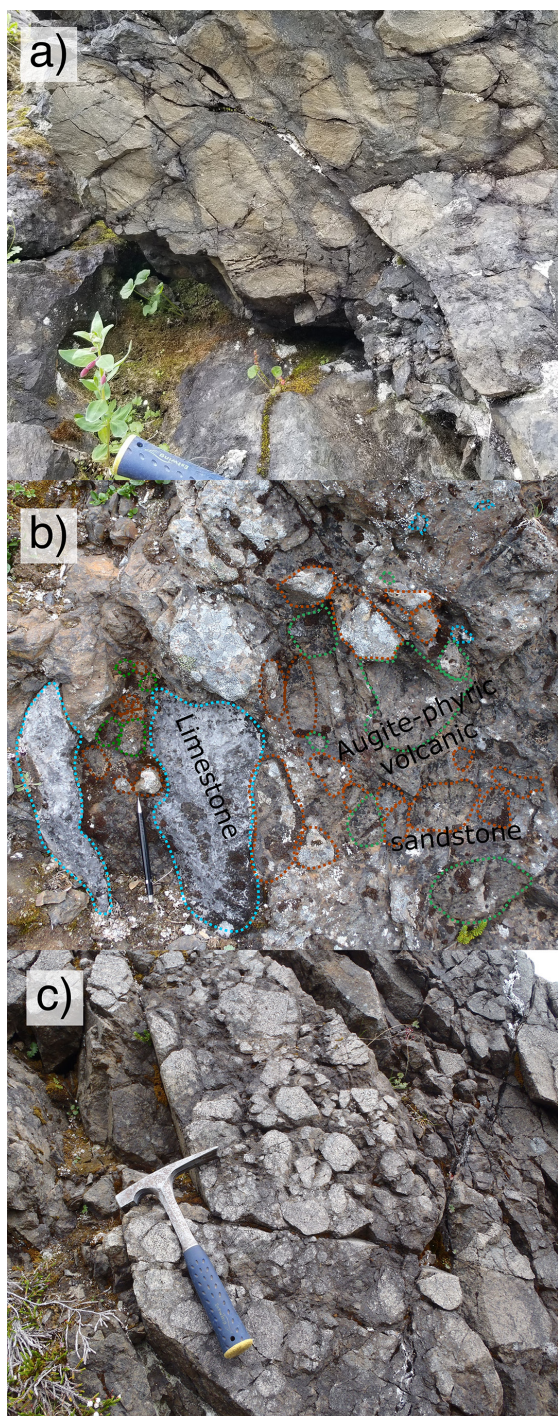


**Fig. 7.** Stuhini-derived Kinskuch conglomerates (uTrIJs). **a)** Framework-intact monomictic cobble-boulder conglomerate with Stuhini-derived angular to subrounded coarse-grained feldspathic sandstone clasts from near the base of the Kinskuch conglomerates, looking northeast, tops upright to the northeast. Some clasts show fractures that do not exist in matrix. **b)** Framework-intact pebble-cobble conglomerate with Stuhini Group-derived clasts of limestone (with cusped-lobate margins, outlined in blue), augite-phyric volcanic rock (outlined in green), and sandstone (outlined in red) in a matrix of coarse grained feldspathic litharenite. **c)** Framework-intact monomictic cobble conglomerate with angular to sub-rounded Stuhini Group-derived augite-phyric volcanic clasts in a matrix of coarse-grained augite-bearing feldspathic sandstone (uTrIJs<sub>v</sub>).

megaclast breccias; due to the size and concentration of the megaclasts they can be mistaken for in situ bedded layers, unless examined along strike.

The clast composition of the conglomerates varies significantly both vertically and laterally. We divide the Kinskuch conglomerates into two mappable subunits based on clast composition: 1) those containing only sedimentary and augite-phyric volcanic rock clasts (Fig. 7; uTrIJs) and, 2) those containing hornblende-feldspar phyric volcanic clasts, sedimentary rocks, and augite-phyric volcanic rock clasts (Fig. 8 uTrIJs<sub>v</sub>). Clast sorting and size varies vertically and laterally from well-sorted to extremely poorly sorted. Clast shape and angularity vary significantly, with some exposures containing predominantly rounded spherical clasts, and some composed mostly of angular and tabular clasts. Chert clasts range from angular to subangular and are mostly spherical. Limestone clasts are mostly rounded to well-rounded but can have irregular cusped-lobate margins. The volcanic, sandstone, and other sedimentary rocks clasts display a wide range of rounding and sphericity. These features vary gradationally laterally and vertically and are not mappable at a 1:10,000 scale.

Upsection changes in clast compositions, particularly at the Tabletop section (Fig. 4), are interpreted to record progressive erosional stripping into deeper levels of the Stuhini Group. At the base of the section, clasts consist mainly of limestones, sandstones, and lesser argillites, mudstones and cherts, similar to those observed in the uppermost Stuhini Group sedimentary rock unit (uTrSs, Figs. 3, 7a), whereas higher in the section clasts consist mainly of augite-phyric volcanic clasts similar to those in the Stuhini Group volcanic rock unit (uTrSv, Figs. 3, 7c). Augite-phyric clasts also show lateral variation and are both more abundant and observed lower in the stratigraphic section, in the west, closer to the Tabletop fault, than in the east, closer to Kinskuch Lake. In sharp contrast to the evidence of top-to-bottom erosion of the subjacent Stuhini Group section, hornblende-feldspar phyric volcanic clasts, presumably derived from the Hazelton Group, appear above Stuhini-derived conglomerates at the 'central lake' and southern 'Big Bulk' sections, although they also appear to directly overlie the Stuhini Group in the most southern exposures (Fig. 4). Laterally, the most significant map-scale variation in clast composition is that these hornblende-feldspar phyric volcanic clasts are lacking in the northern exposures (Fig. 4).

#### 4.2.1.1. Megaclast deposits

Some of the conglomerates contain megaclasts up to 120 m long. The megaclasts consist mostly of limestone (Fig. 10a) and laminated chert (Fig. 10b) with laminations parallel to original bedding planes. Megaclasts of thinly bedded sedimentary rocks (up to 75 m long, Figs. 10c, d) and augite-phyric volcanic rocks (up to 5 m long) are less common. The chert megaclasts commonly display an internal fracture network with jig-saw fit, suggesting fragmentation with minimal relative movement during transport; locally, megaclasts of chert contain internal

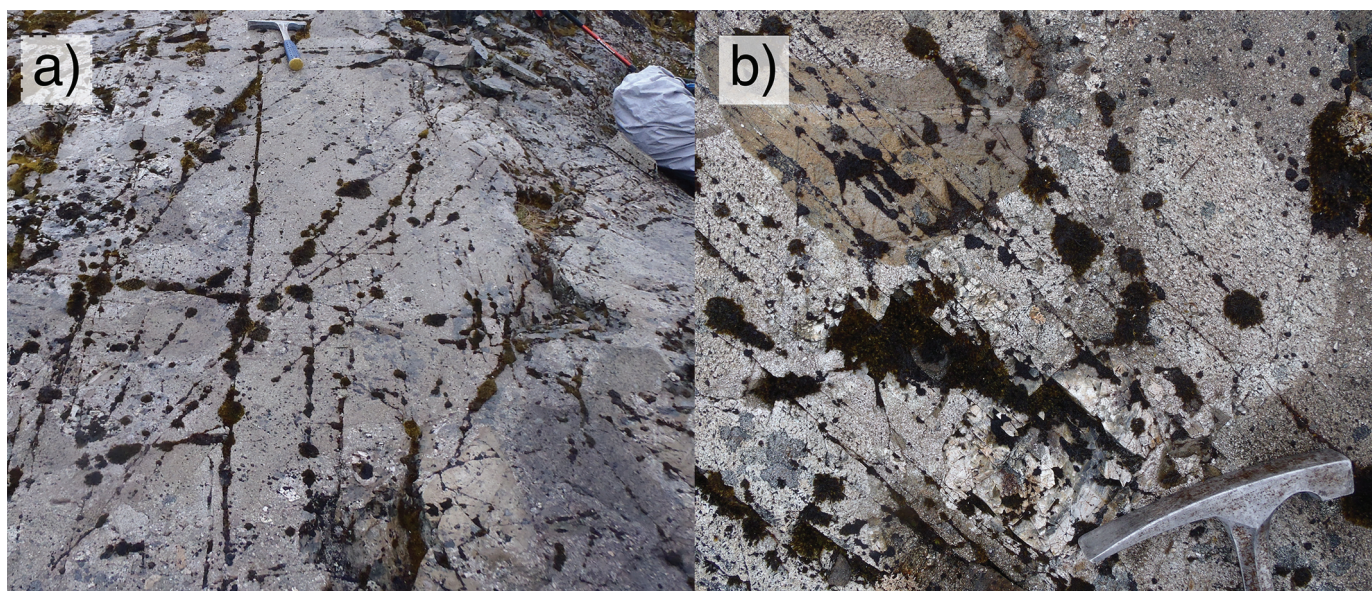


**Fig. 8.** Stuhini- and Hazelton-derived Kinskuch conglomerates (uTrlJh). **a)** Matrix-supported pebble to boulder conglomerate with angular pebble to cobble chert clasts, rounded pebble to boulder Stuhini-derived sandstone clasts and well-rounded cobble to boulder hornblende-phyric Hazelton Group-sourced clasts in a coarse-grained feldspathic litharenite matrix (uTrlJhs). Looking northwest, tops to northwest. **b)** Detail of above, showing hornblende-phyric Hazelton Group-sourced and Stuhini Group-sourced sandstone and chert clasts.

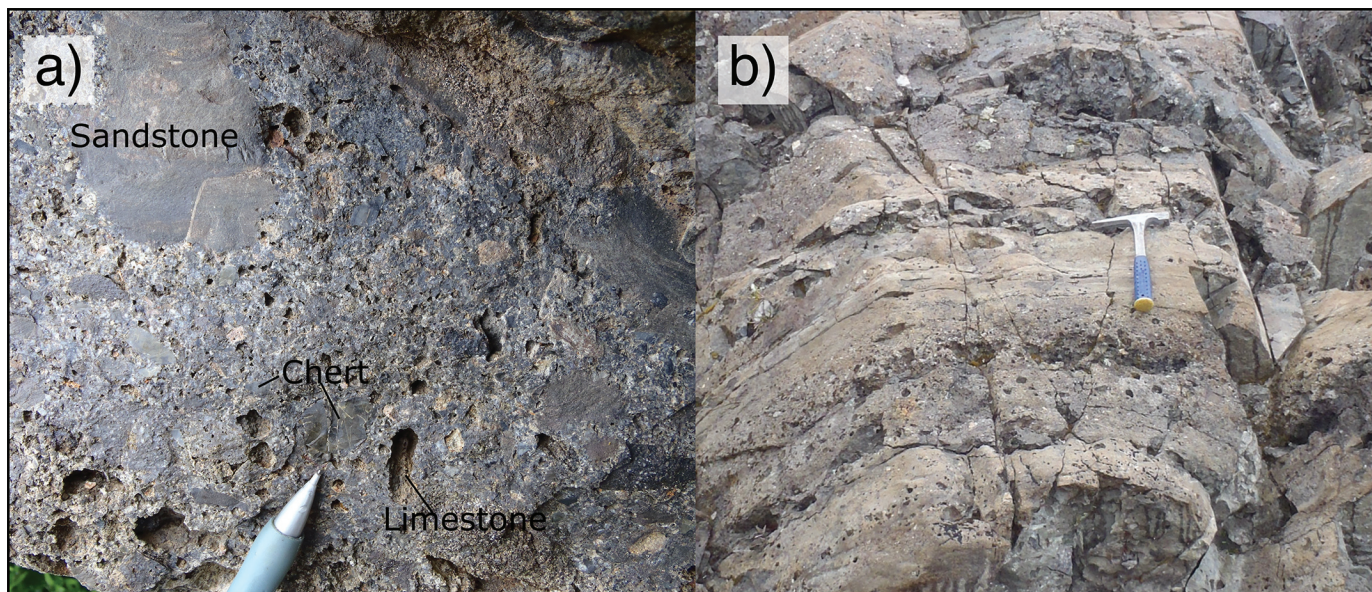


**Fig. 9.** Mainly pebble Kinskuch conglomerates from the central lake area. **a)** Clast-supported pebble to rare cobble conglomerate with rounded to angular chert clasts, recessively weathering lobate limestone clasts, rounded to subangular sandstone clasts, and rare feldspar-phyric volcanic clasts. **b)** Fining-upward sequences of pebble conglomerate to pebbly litharenite to feldspathic arenite to siltstone; looking northeast, tops northeast.

folds that are truncated at clast boundaries (Fig. 10b). The matrix of the megaclast-bearing conglomerates is composed of coarse-grained lithic arkose to litharenite with no quartz. Along the margins of some megaclasts, monomictic cobble to pebble breccia commonly grades into a more polymictic conglomerate, indicating derivation from less local sources. The matrix surrounding the megaclasts is generally massive.

Locally, megaclast fragments are separated by little intervening matrix and may be confused with in situ protolith.

Non-systematic changes in bedding and younging direction in these bodies indicate that they are clasts. In one exposure, near the Big Bulk prospect, thinly bedded sedimentary megaclasts in a megaclast-supported breccia that is interbedded with coarse-grained sandstones have abundant soft-sediment deformation structures including sandstone and mudstone dikes (Figs. 10c, d).

The megabreccias are most prominent at the base of the Kinskuch conglomerate unit (Fig. 4), but they also occur higher

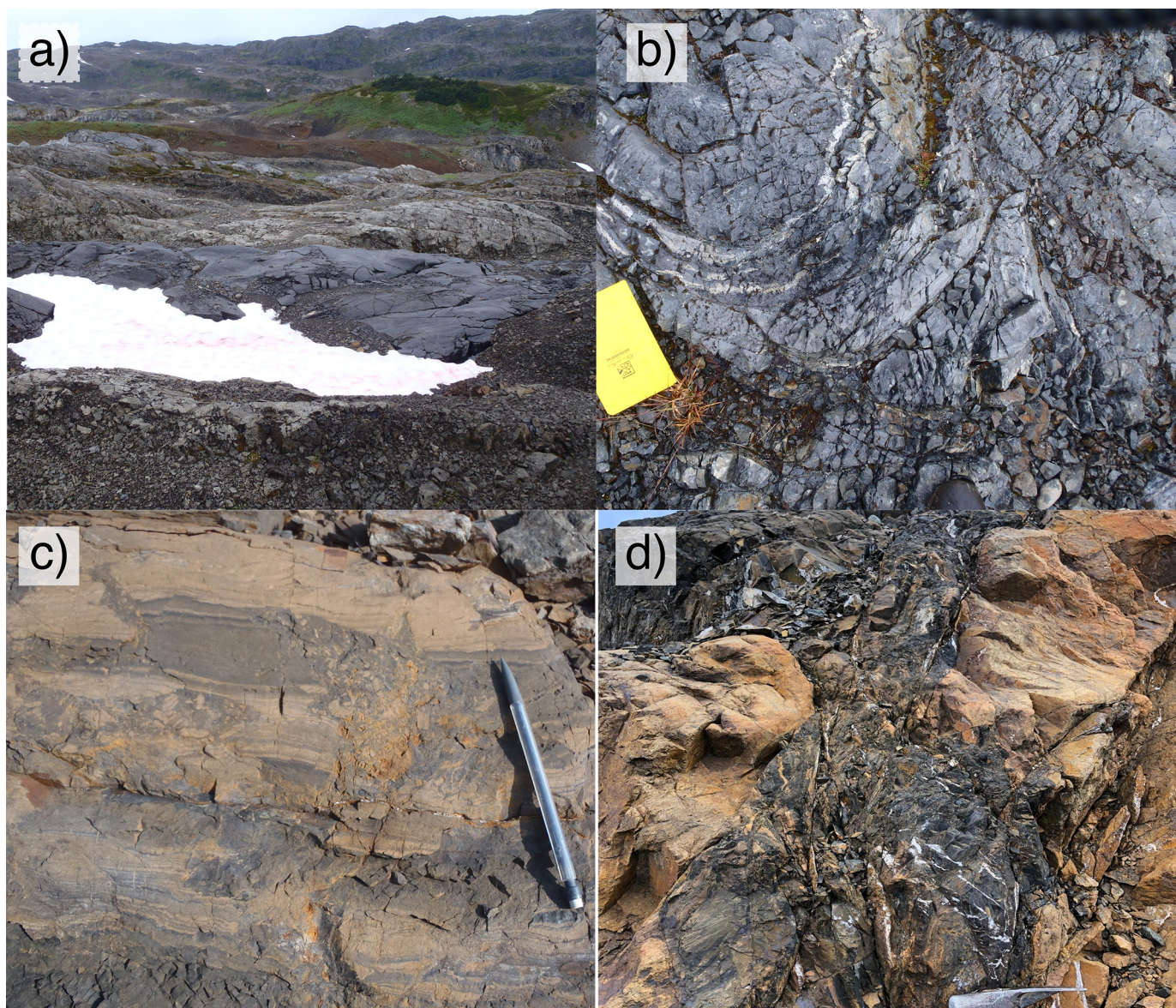


**Fig. 10.** Megaclast-bearing Kinskuch conglomerates **a)** Dark grey-weathered limestone megaclast in framework-intact clast-supported cobble to boulder conglomerates with fractured subangular to subrounded sandstone, chert and limestone clasts. View to the northwest, tops northwest. **b)** Chert megaclast with internal fold that predates jig-saw fit fracturing and incorporation into the conglomerates. **c)** Megaclast of thinly bedded orange-weathering feldspathic arenite and dark mudrock with soft-sediment deformation structures, including sandstone and mudstone dikes. **d)** Megaclast-supported conglomerate with coarse-grained sandstone megaclasts and disrupted megaclasts of finely bedded dark grey argillites and minor orange-weathering sandstone interbeds.

in the section, including directly beneath Hazelton Group volcanic rocks in the southern part of the map area, near the Big Bulk stock. They are most abundant, particularly at higher stratigraphic levels in the northern and southern parts of the map area (Figs. 3, 4).

Cordey et al. (1992) and Greig et al. (1992) collected conodonts from a limestone exposure that we consider a  $\geq 100$  m megaclast near the base of the Kinskuch conglomerate unit. These conodonts, originally interpreted as Late Norian, are now assigned to the Rhaetian (Golding et al., 2017; M. Golding, pers. comm., 2019), providing a maximum age for the Kinskuch conglomerates. Hunter and van Straaten (2020)

report a maximum depositional age from detrital zircons (U-Pb, LA-ICPMS) of  $206.7 \pm 1.9$  Ma (Rhaetian) for the onset of Hazelton Group volcanism and below we provide an U-Pb zircon CA-TIMS age of  $204.61 \pm 0.18$  Ma for phase 2 of the Big Bulk stock, which cuts basal Hazelton Group rocks. Hence, unroofing of the Stuhini Group, and the tectonics it implies, started in the Rhaetian.

#### 4.2.2. Hazelton Group (Upper Triassic-Jurassic) volcanic-sedimentary sequences (IJHvs, IJHv)

Hornblende-feldspar phyric volcanic breccias of the lower Hazelton Group (IJHv) are exposed on the east and south

sides of Kinskuch Lake and on the ridge west of the Tabletop fault. Locally, in the central part of Kinskuch Lake and east of the Tabletop fault, the base of the sequence is marked by hornblende-feldspar-rich crystal tuffs interstratified with siliciclastic sedimentary rocks (IJHvs). Southeast of the Tabletop fault, near Kinskuch Lake, these strata overlie the Kinskuch conglomerates, whereas northwest of the Tabletop fault, hornblende-feldspar volcanic breccias are in direct contact with Stuhini Group sedimentary rocks along a very low angle unconformity and intervening Kinskuch conglomerates are absent (Figs. 3, 4).

#### 4.2.2.1. Siliciclastic sedimentary rocks with hornblende-feldspar crystal tuff

On the west side of Kinskuch Lake, unit IJHvs consists of pale-weathering, well-stratified to locally massive, coarse-grained feldspathic sandstone to siltstone with lesser pebble conglomerate, angular hornblende-feldspar-rich medium-to-coarse-grained sandstones and mudstone interstratified with hornblende-feldspar crystal tuff. The pebble conglomerates are polymictic, containing variably rounded to angular clasts of chert, argillite, sandstone, augite-phyric volcanic rocks and lesser hornblende-phyric volcanic rocks, with a wide range of sphericity, similar to the underlying Kinskuch conglomerates. Quartz is not present in any rocks. The sandstones locally show cross bedding and grading. Where this unit is exposed on Tabletop mountain, tuff interlayers are thin (0.5-10 cm) and comprise a maximum of 10% of the rock volume (Fig. 11a).

In the west-central part of the map area tuff beds are 10-40 cm thick and consist mainly of grain-supported, very coarse hornblende and feldspar (Fig. 11b). Several polymictic pebble conglomerates and pebbly sandstones (both containing clasts of limestone, thinly bedded feldspathic sedimentary rocks, and minor chert like those in the underlying Kinskuch conglomerates) are interstratified with these tuffs, suggesting a gradational, conformable contact. The base of the volcanic-sedimentary unit is defined as the first appearance of the tuff.

#### 4.2.2.2. Andesitic volcanoclastic breccia (IJHv)

This unit consists of monomictic to locally polymictic agglomerate containing large (5-30 cm, rarely >50 cm), angular to subrounded hornblende-feldspar-phyric juvenile blocks and bombs. The breccia is matrix- to clast-supported (30-50% clasts); in some cases clasts are more strongly epidote-chlorite altered than surrounding groundmass or show rims suggesting partial resorption. The unit also includes tuff breccia and minor lapillistone with a distinctive hornblende and feldspar crystal-rich matrix (Fig. 11c). Rare feldspar±hornblende crystal tuffs and crystal-rich, volcanic-derived sandstones, with limited strike extent, are locally exposed. The volcanic rocks are cut by rare channels filled with coarse sandstones. Minor sandstone, limestone, argillite and rare augite-phyric volcanic accessory clasts are generally only observed within fifty metres of the contact with underlying Stuhini Group rocks, where they may comprise up to 30% of the clast population. They are commonly

moderately to strongly chlorite-epidote altered and range from well rounded to subangular (Fig. 11d).

### 4.3. Intrusive rocks

#### 4.3.1. 'Big Bulk stock' (latest Triassic)

The Big Bulk stock is a multiphase hornblende diorite porphyry that cuts most of the stratified rocks in the map area. Based on crosscutting relationships, we have subdivided it into four phases. Contacts between the phases generally trend east-west. Phases 2 and 3 are locally separated by an intrusive breccia unit consisting of flow-banded hornblende diorite porphyry.

##### 4.3.1.1. Phase 1: Hornblende diorite with accessory magnetite

Phase 1 diorite is the most voluminous by mapped surface exposure and predominates on the north side of the stock. It is a crowded diorite containing approximately 15-20% plagioclase phenocrysts (1-2 mm) and 10-15% hornblende phenocrysts (2-3 mm) in a predominantly fine-grained (<1 mm) groundmass consisting primarily of plagioclase, hornblende, and accessory magnetite. Unlike subsequent phases, it does not contain diorite or vein xenoliths, but commonly contains country rock xenoliths close to external contacts. Phase 1 diorite is locally cut by minor (up to 5%) pyrite and quartz veins including quartz-magnetite±chalcopyrite veins. Veins are most abundant at the southern extent of the phase 1 exposure and are largely absent in the north. Exposures in the northwest have weak chlorite-sericite replacement of hornblende and exposures in the east locally display nearly complete quartz-sericite-pyrite replacement.

##### 4.3.1.2. Phase 2: Quartz-chalcopyrite veined hornblende diorite porphyry

Phase 2 diorite is the least voluminous phase, based on surface exposure, and is surrounded by later phases. It is exposed primarily as two east-west trending bodies with a maximum width of 100 m. Small (10-50 m), isolated bodies of phase 2 are also exposed in the east, in phase 3 rocks. Phase 2 diorite is texturally and mineralogically similar to phase 1. It is moderately biotite-chlorite-magnetite altered (primarily replacing hornblende) with a weak to intense quartz-sericite-pyrite overprint. Quartz-sericite-pyrite alteration is commonly strongest near phase 3 contacts or close to faults.

Phase 2 is the most strongly mineralized phase and characteristically contains significant sheeted quartz-chalcopyrite±bornite±pyrite veins (Fig. 12) commonly forming an orthogonal set (Fig. 13a). The mineralized quartz veins make up 20 to 45% of the rock mass. Pyrite veins and veinlets (<1 cm wide) are locally abundant, spatially correlated with increasing quartz-sericite-pyrite alteration, and cut the quartz-chalcopyrite veins. Phase 2 contains 5% small (0.5-2 cm) xenoliths of hornblende diorite that resemble both phase 1 and phase 2 in mineralogy and texture. The xenoliths have the same alteration assemblage and intensity as the phase 2 diorite and were altered

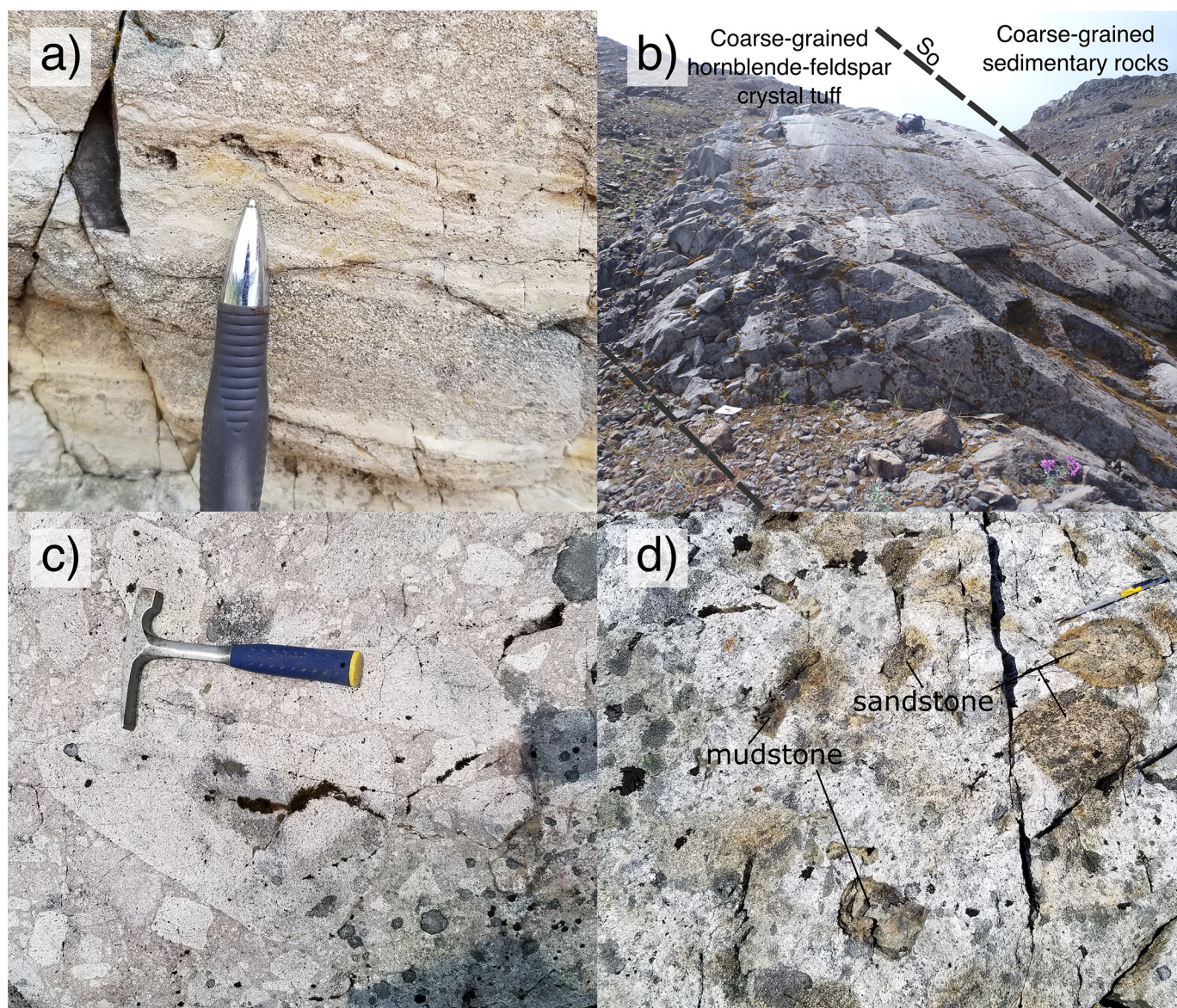


**Fig. 11.** Hazelton Group volcanic and sedimentary rocks. **a)** Interbedded sandstone, siltstone, and feldspar-crystal tuff younging upright, looking NE. **b)** Coarse-grained hornblende-feldspar crystal tuff interstratified with coarse-grained feldspathic sandstones and polymictic pebble conglomerates, looking northwest tops to the north. **c)** Monomictic volcanic breccia with angular poorly sorted juvenile lapilli to bombs of hornblende-feldspar-phryic intermediate volcanic rock in a similarly composed groundmass. **d)** Volcanic breccia containing juvenile hornblende-feldspar-phryic volcanic blocks and lesser Stuhini Group-derived accessory clasts.

after being incorporated. A sample of phase 2 diorite returned a preliminary U-Pb zircon CA-TIMS age of  $204.61 \pm 0.18$  Ma (see below).

#### 4.3.1.3. Flow-banded hornblende diorite porphyritic intrusive breccia

An intrusive breccia cuts phase 1 and phase 2 diorites in exposures directly south of Kinskuch Lake. Although it is compositionally similar to other phases it is texturally distinct, with a wider range of phenocrysts, including 2% to locally 15% feldspar and 1% to locally 10% hornblende in a very fine-grained, dark green, strongly chlorite to sericite-pyrite-altered flow-banded groundmass (Fig. 14a). The breccia zone contains

between 10-30% xenoliths of hornblende diorite (1-30 cm), and lesser quartz=chalcopyrite vein fragments (1-2 cm). Some diorite xenoliths are much more intensely and variably altered than the groundmass, ranging from weakly to intensely quartz-sericite-pyrite altered, moderately chlorite-pyrite±sericite altered, to nearly unaltered, and some are cut by quartz-chalcopyrite veins that terminate at xenolith boundaries. Thus we infer that these xenoliths have undergone some alteration and porphyry-style veining before, or during incorporation into the intrusive breccia.

Locally, several small (1-3 m wide) clast-rich intrusive breccia and lesser quartz-cemented breccia pipes with steep east-west trending contacts cut the main, flow-banded intrusive

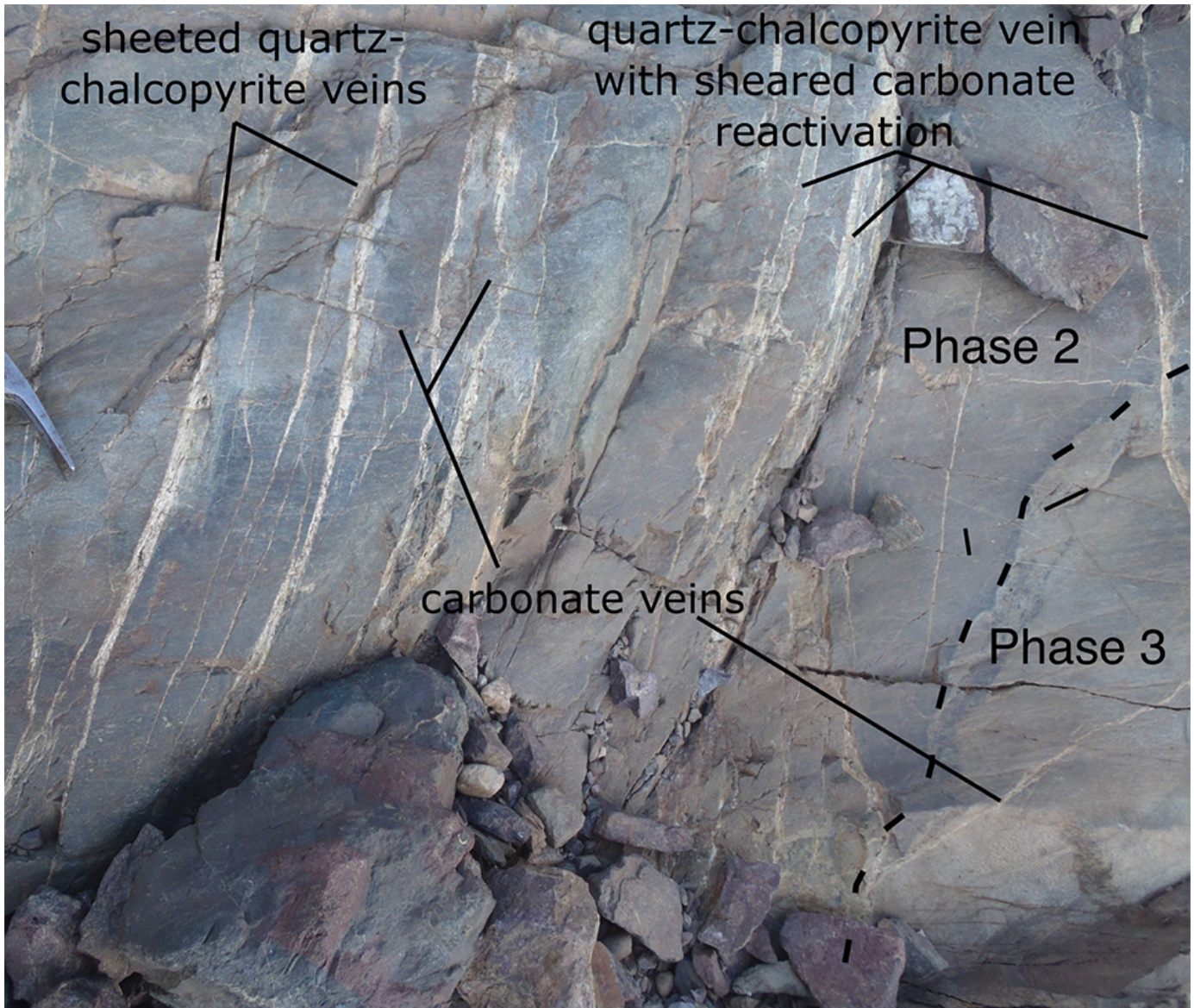


**Fig. 12.** Phase 2 Big Bulk hornblende diorite cut by phase 3 diorite. East-west oriented sheeted quartz-chalcopyrite veins of stage 2 mineralization in phase 2 diorite cut by thin (1-2 mm) carbonate veins. Some Stage 2 veins have carbonate cores or borders that indicate reactivation by post-mineral fluids. Top of photo is to the east.

breccias (Fig. 14b). They are not observed cutting any other phases. These small breccia pipes contain up to 50% variably altered and mineralized diorite clasts and quartz veins similar to the intrusive breccia that they cut. Very rarely, the matrix of the breccias consists of chalcopyrite-bearing quartz.

#### 4.3.1.4. Phase 3: Hornblende diorite porphyry

Phase 3 diorite is the second most voluminous phase, based on surface exposure. It cuts phase 1, phase 2 and the intrusive breccia and has sharp east-west trending contacts commonly displaying chill margins and ripped up xenoliths of the earlier phases (Fig. 12). Most quartz-chalcopyrite veins in phase 2 diorites are abruptly cut at contacts observed with phase 3. Xenoliths of Stuhini Group and Hazelton Group country rock up to 4 m long are common within about 50 m of a contact.

In its southwestern-most exposure, several dikes and sills (1-6 m wide) of phase 3 diorite intrude the surrounding bedded sedimentary rocks. The country rock in contact with phase 3 diorites is often moderately to strongly sericite-pyrite altered.

Although mineralogically and texturally similar, phase 3 is distinguished from phases 1 and 2 primarily by the scarcity of intact quartz-chalcopyrite veins (less than 2%), and the occurrence of fragmented quartz-chalcopyrite veins, and quartz-chalcopyrite veined diorite xenoliths (1-5%). The xenoliths are variably altered (predominantly weakly to strongly quartz-sericite-pyrite=chlorite with lesser moderately chlorite altered) and in most cases are more strongly altered than the diorite into which they are incorporated. Phase 3 is cut by abundant (up to 20%) stockworked pyrite veins and veinlets, most of which are less than 0.5 cm wide, although some can be as wide as 10 cm

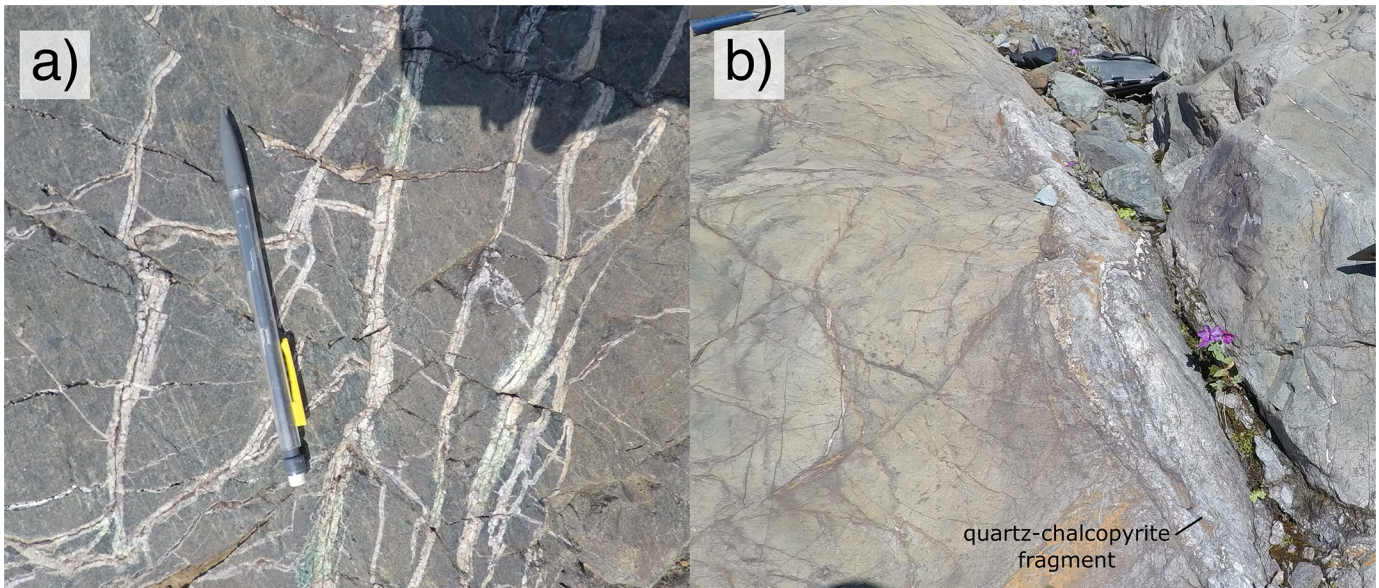


**Fig. 13.** Big Bulk stock stage 2 (main mineralization) and stage 3 (late mineralization) veins. **a)** Phase 2 hornblende diorite porphyry, with characteristic stage 2 sheeted to orthogonal quartz-chalcopyrite veins with sulphide-rich centres. Recessively weathering carbonate veins cut and offset porphyry related veins. **b)** Phase 3 hornblende diorite porphyry with moderate quartz-sericite-pyrite (phyllic) alteration and abundant stockworked stage 3 pyrite veins, cut by a large laminated iron-carbonate vein with sheared and brecciated quartz-chalcopyrite and massive sulphide vein fragments.

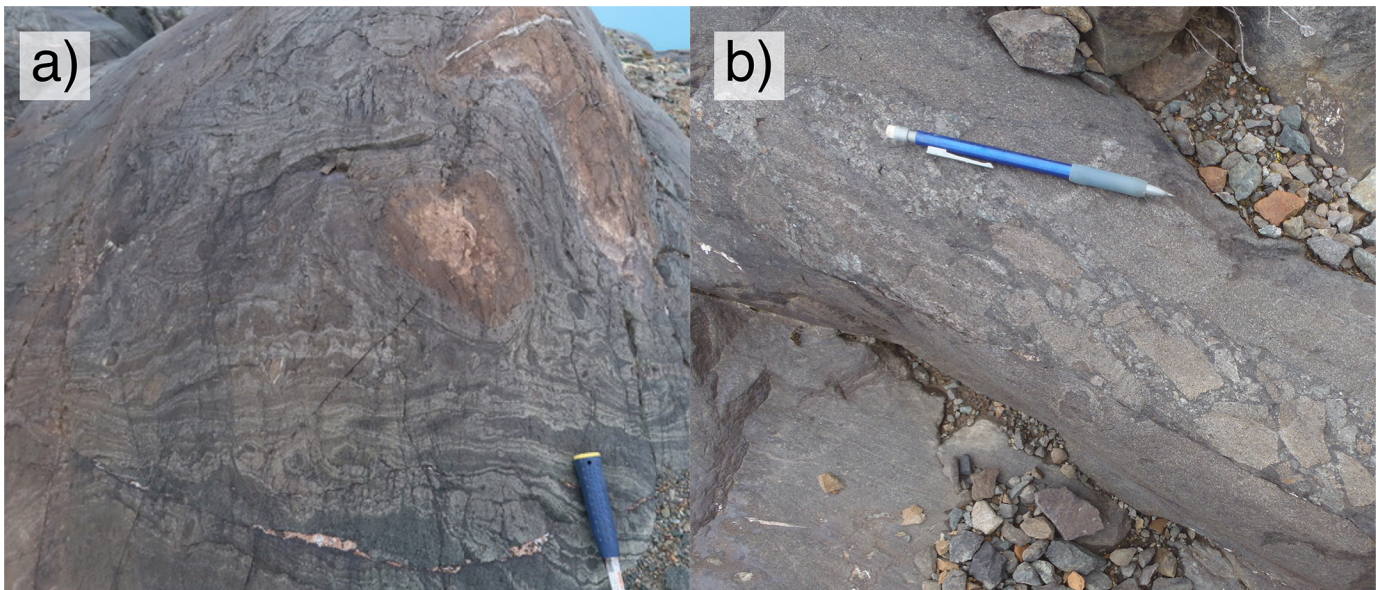


**Fig. 14.** Big Bulk stock intrusive breccia. **a)** Fine-grained chlorite-sericite altered flow-banded intrusion breccia with xenoliths of variably altered diorites and veins. **b)** Clast-supported intrusive breccia pipe cutting main intrusive breccia.

(Fig. 13b). These pyrite veinlets cut xenoliths and contacts between phase 3 and Phase 2 diorites.

#### 4.3.1.5. Phase 4: Biotite-hornblende monzodiorite to monzonite

Phase 4 is the most mineralogically and texturally distinct of the Big Bulk phases. It is an equigranular to weakly hornblende porphyritic fine- to medium-grained hornblende±biotite monzodiorite to monzonite. It cuts phase 3 at the southern margins of the Big Bulk stock with sharp intrusive contacts.

The contacts are commonly visible from a distance, marked by an abrupt decrease in alteration from the rusty weathering of pyrite-rich phase 3 to grey to green weathering of phase 4. Phase 4 monzodiorites are mostly unaltered with local weak to moderate chlorite±epidote alteration of hornblende. Weak quartz-sericite-pyrite alteration, with at most 2% disseminated pyrite, is locally observed close to crosscutting faults. It contains rare (<2%) xenoliths of quartz-chalcopyrite vein-bearing and strongly quartz-sericite-pyrite altered diorites but is otherwise unmineralized.

#### 4.4. Late dikes (Eocene?)

Two distinct suites of nearly unaltered dikes, thought to belong to the Eocene Hyder suite, cut all Triassic-Jurassic rocks and reverse faults in the map area. They are locally offset by steep, dextral brittle faults with m-scale displacement. The two suites display similar orientations: steep to subvertical trending roughly north-south or east-west, and are traceable for up to 1 km along strike. Intermediate biotite-hornblende-feldspar porphyry dikes and stocks are the most prominent and are up to 10 m wide. They contain fine- to medium-grained lathes and needles of hornblende and feldspar in a very fine-grained groundmass. The second suite are dark green to brown weathering mafic dikes up to 5 m wide. They are aphanitic with rare very fine-grained hornblende±feldspar needles as phenocrysts, or calcite-filled amygdules.

#### 5. Structure

The most prominent structures in the Kinskuch Lake area are northerly trending faults and folds (Figs. 3, 15). The map-scale faults are typically expressed as pronounced lineaments (Figs. 16a, b). The east side of Kinskuch Lake has abundant moderately to shallowly, generally west- to northwest-dipping imbricated thrust faults (Figs. 3, 16c) that cut all Triassic to Jurassic units, porphyry related-veins and alteration in the map area. The thrust faults are commonly lined with sheared iron-carbonate±calcite±barite veins and clasts (Fig. 16d), similar to other faults in the region considered to be Cretaceous (see Febbo et al., 2019). Folds related to thrust faults have northeast-trending hinge lines, moderately west-dipping axial surfaces and verge to the east, commonly with overturned eastern limbs (Fig. 15).

In the western part of the map area, the faults are primarily steeply dipping, mainly northeast-trending dextral strike-slip structures such as the Tabletop fault, and east-trending, steeply dipping, south-side-up and north-side-up oblique-slip faults, such as the 'central lake fault' (Fig. 3). Folds with m-scale wavelengths and east-west striking, moderately dipping axial surfaces are spatially associated with east-trending faults.

Most of the map-scale folds are asymmetric, tight to open, inclined steeply to moderately to the west, and doubly plunging. Many of the map-scale folds are associated with faults, with axial traces oriented northeast-southwest near Tabletop fault to nearly north-south to northeast-southwest in the central lake area (Fig. 3). Minor, m- to dm-scale tight folds are restricted to fine-grained sedimentary units, commonly paired with minor faults with similar orientation to larger scale folds. These folds are rounded and typically have strongly fractured hinges and axial planar faults. In calcareous rocks, calcite veins are common in the hinge zones. Broad open northeast-trending folds west of the Tabletop fault (Figs. 3, 15a) have axial traces that are oblique to the fault, consistent with dextral strike slip.

Axial planar cleavage is only locally developed as a spaced fracture cleavage in fine-grained sedimentary rocks and absent in most other rock types. However, cleavage is well-developed in strongly phyllic-altered rocks in the Big Bulk deposit. Shear

zones, especially in strongly quartz-sericite-pyrite altered rocks in the Big Bulk deposit (Fig. 16c) also have well-developed foliation.

#### 6. Geochronology: Big Bulk stock, phase 2

We collected a sample of the Big Bulk stock phase 2 diorite for U-Pb single-zircon chemical abrasion thermal ionization mass spectrometry (CA-TIMS) geochronology. The analytical work was carried out by Richard Friedman at the Pacific Centre for Isotopic and Geochemical Research (University of British Columbia); detailed methods and results will be presented elsewhere. Preliminary results indicate a young concordant group of zircons that are tentatively interpreted as primary magmatic grains recording a crystallization age of 204.61 ±0.18 Ma (Fig. 17; Table 1). Intriguingly, three of the eight grains analyzed yielded concordant Paleozoic <sup>207</sup>Pb/<sup>206</sup>Pb ages (ca. 456-400 Ma) ages. Likely xenocrysts, these older grains provide a window into the nature of basement to Stikinia.

#### 7. Mineralization, and veins at the Big Bulk prospect

##### 7.1. Stage 1: Early mineralization

The earliest porphyry-related veins recognized are mutually crosscutting quartz-magnetite±chalcopyrite±pyrite veins (0.5-1 cm wide) and lesser braided magnetite veinlets (<1 mm) with 1-2 mm wide magnetite-quartz alteration selvages. Both vein types are rare, making up at most 2% of the rock volume. The quartz veins have fine-grained magnetite and sulphide-rich centres. These veins are in phase 1 and 2 diorites and rarely in Hazleton Group volcanic rocks in contact with phase 1 diorites. They are cut by all other vein types.

##### 7.2. Stage 2: Main-phase mineralization

Stage 2 is marked by moderate to strong quartz-sericite-chlorite-biotite alteration and rare potassic feldspar. Remnant secondary biotite is generally only recognizable where later stages of alteration are very weak. Stage 2 veins contain quartz-chalcopyrite±pyrite±bornite and have sulphide-rich centres. Stage 2 veins occur as steeply dipping, sheeted veins (Fig. 12) or form orthogonal sets with northwest and east-northeast trends (Figs. 13a, 18a). Stage 2 veins typically have sharp, planar contacts, but are locally discontinuous and tightly anastomosing, with diffuse boundaries. Stage 2 veins cut phase 1 and 2 diorites. In phase 3 diorite, quartz-chalcopyrite veins occur mostly as xenoliths with few quartz-chalcopyrite veins, suggesting that only minor main-mineralizing phase fluid circulation persisted after intrusion of phase 3 diorites. Quartz-chalcopyrite veins occur as, or within, rare xenoliths within phase 4 monzodiorites.

##### 7.3. Stage 3: Late stage-mineralization

Pyritic veinlets (<1 mm) and veins (1-10 cm) cut stage 1 and stage 2 veins and are associated with strong to intense quartz-sericite-pyrite (QSP) alteration that is commonly pervasive and mineralogically and texturally destructive. They cut all Big Bulk phases, except the phase 4 monzodiorites, and are

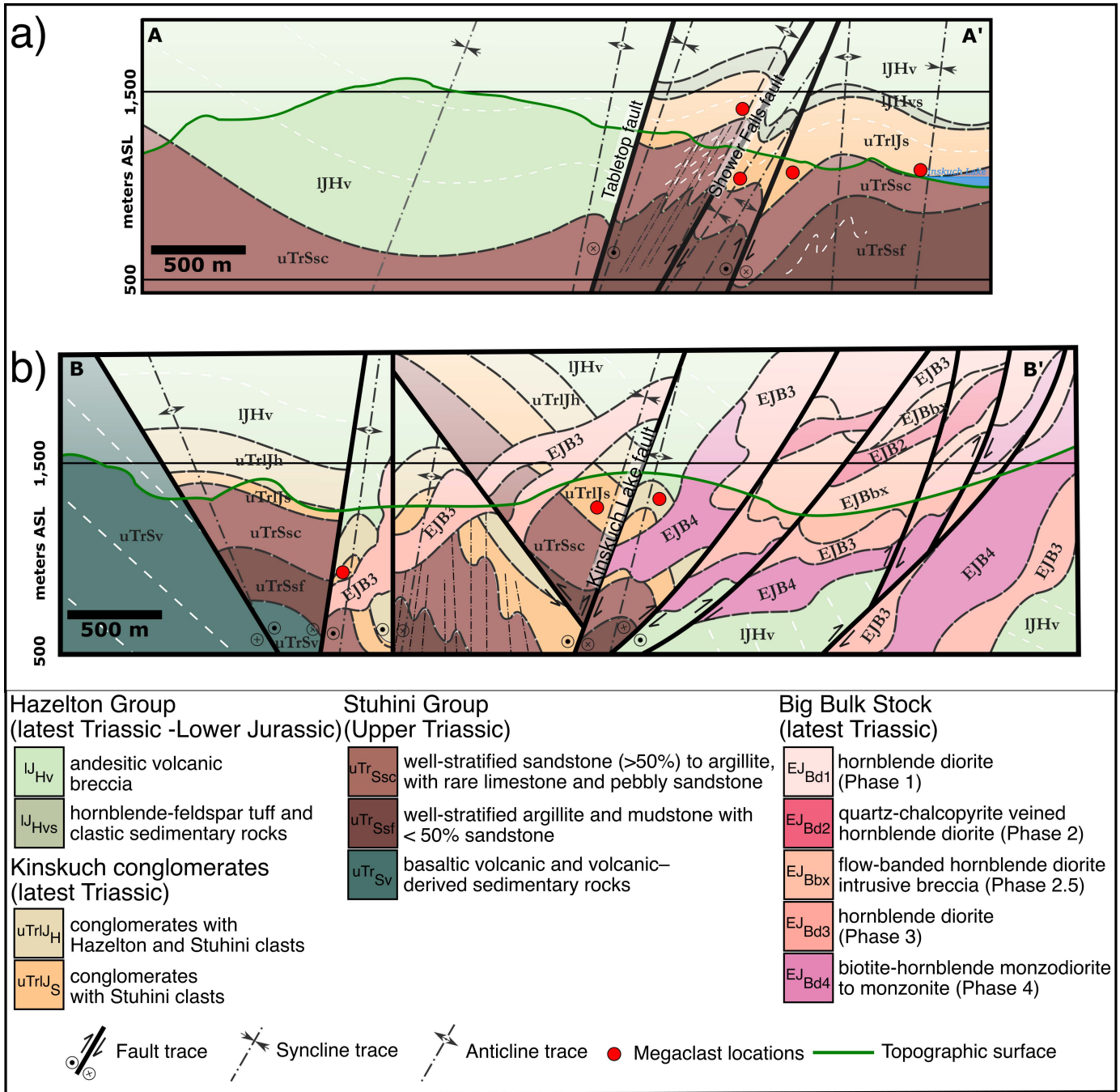


**Fig. 15.** Structural cross sections (see Fig. 2 for locations). **a)** Section A-A' shows paired faults and folds typical on the western side of the lake. The transitional conglomerates are only developed east of the Tabletop fault; to the west hornblende-feldspar Hazelton Group volcanic breccias are in direct contact with Stuhini Group sedimentary rocks along a very low angle unconformity and intervening transitional conglomerates are absent. **b)** Section B-B' shows the transition from paired folds and faults in stratified units in the west to the imbricate thrust-faulted and tilted Big-Bulk stock to the east.

particularly abundant in and surrounding phase 3 diorites (up to 20%). The veins range from planar to anastomosing and generally form stockworks (Fig. 13b).

**7.4. Post-mineral veins**

Iron-carbonate±barite and calcite veins (0.2-30 cm wide) are common in the map area and cut all Triassic and Jurassic units as well as all stage 1 through 3 veins (Fig. 13).

**8. Discussion**

**8.1. Latest Triassic to Early Jurassic tectonics and sedimentation**

The Kinskuch conglomerates mark a fundamental break in the tectonic history of the region. Thick conglomeratic sections demand topographic relief to expose source rocks to erosional levels and create accommodation space for preservation. This relief is best generated by syndepositional faults. The megaclast-

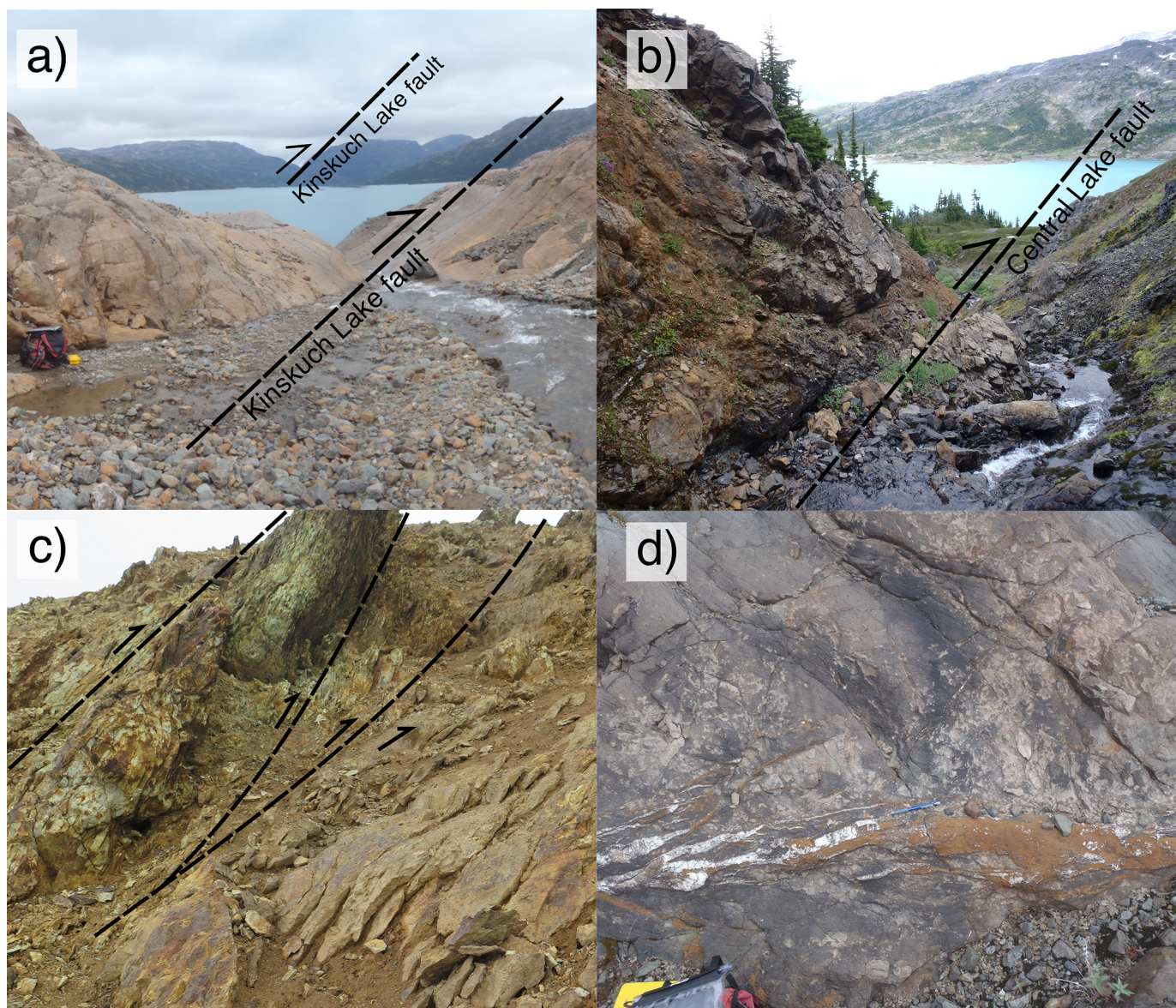


**Fig. 16.** Typical faults in the map area. **a)** View to the north of the northeast-trending, moderately west-dipping Kinskuch Lake thrust fault cutting Big Bulk diorite. **b)** View to the east of the east-trending central lake fault, which juxtaposes coarse-grained well-stratified sandstone southward above megaclast-bearing Kinskuch conglomerate containing mainly Stuhini Group-derived clasts. **c)** Thrust imbricates in intensely quartz-sericite-pyrite altered hornblende diorite (Big Bulk stock phase 3) with well-developed cleavage. **d)** Iron-carbonate fill spatially related to east-vergent reverse faults on the eastern side of the map area.

bearing conglomerates are particularly significant and were likely deposited immediately adjacent to syndepositional fault scarps. Progressive stripping to deeper parts of the subjacent Stuhini Group section, as recorded by bottom-to-top clast compositions that yield an inverse stratigraphy, signifies approximately 400 m or more, of Stuhini Group unroofing (Figs. 19, 20). Conodonts recovered from a limestone megaclast derived from the Stuhini Group are Rhaetian, providing a limit to the onset of faulting. Faulting continued during deposition of the Hazelton Group, as indicated by intraformational clasts and by interbedding of the conglomerates and basal Hazelton tuffs. The onset of Hazelton Group volcanism in the area is constrained by a U-Pb detrital zircon maximum depositional

age of  $206.7 \pm 1.9$  Ma (Hunter and van Straaten, 2020) from rocks a few km north of Kinskuch Lake. Phase 2 of the Big Bulk stock, which cuts the basal Hazelton Group, has a U-Pb zircon crystallization age of  $204.61 \pm 0.18$  Ma (this paper). Thus, like elsewhere in northwestern Stikinia (see below), the Rhaetian (ca. 208-201 Ma; Cohen et al., 2013) witnessed the demise of the Stuhini arc and a major tectonic and magmatic reorganization.

The conglomerates are notably absent west of the Tabletop fault, leading us to suggest that it is a long-lived structure with an early southeast-side down history that led to unroofing of the Stuhini Group. Furthermore, the large megaclasts of limestone and chert are found close to the present position of east-west

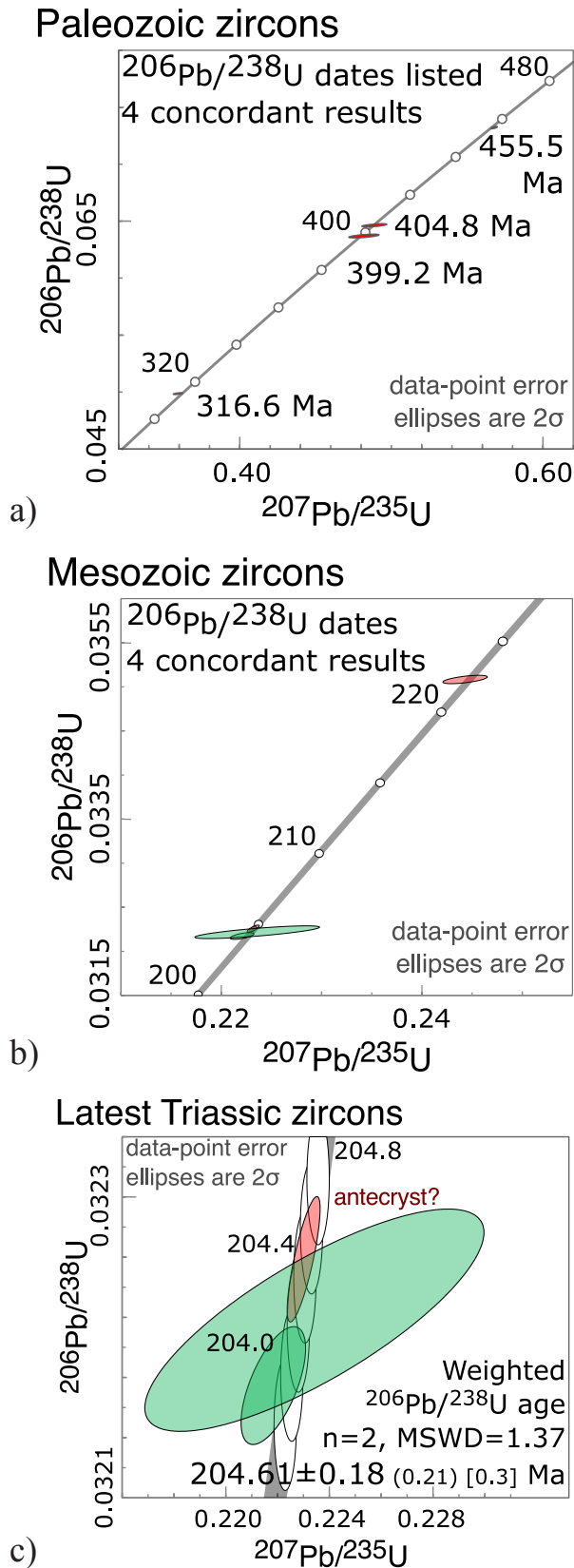


**Fig. 17.** Concordia plots for CA-TIMS U-Pb analysis of zircons from phase 2 diorite of the Big Bulk stock. **a)** Paleozoic xenocrystic grains. **b)** Mesozoic xenocrystic grains. **c)** Latest Triassic grains yielding a preliminary crystallization age of  $204.61 \pm 0.18$  Ma.

trending faults (e.g., ‘shower falls’ and ‘central lake’; Figs. 3, 19), and we speculate they too may have been active during sedimentation to generate significant topographic relief. If so, younger Cretaceous fold and thrust belt deformation has reactivated, inverted, and likely reoriented many of the faults that would have been active during this time, obscuring original kinematics and displacement. We propose that the Tabletop fault and likely other northeast-trending faults in the area had an early (latest Triassic) history with strike-slip or oblique movement, and that releasing step-overs, splays, or double bends in this fault network created local zones of north-south extension, easterly trending normal faults, and local pull-apart basins into which the Kinskuch conglomerates were deposited. Consistent with the notion of local north-south extension and east-west trending normal faults, the Big Bulk phases of intrusion are more or less tabular, with an overall east-west orientation, and the sheeted veins of the main stage porphyry also have an east-west orientation.

## 8.2. Regional tectonic and metallogenic implications

Similar evidence for latest Triassic to Early Jurassic syndepositional faulting and deposition of conglomeratic rocks has been reported in the KSM and Bronson areas (Nelson and Kyba, 2014; Kyba and Nelson, 2015; Febbo et al., 2019), suggesting widespread, latest Triassic tectonic instability throughout much of the Stewart-Iskut district during the transition from the Stuhini Group to the Hazelton Group. This transition appears to be broadly coeval with latest Triassic to Early Jurassic deformation in the Stewart-Iskut district (e.g., Logan and Koyanagi, 1994; Brown et al., 1996) and is also broadly coeval with uplift and erosion of Stikine plutonic suite batholiths (Late Triassic; Brown et al., 1996; van Straaten and Nelson, 2016). U-Pb detrital zircon studies show that erosion of these batholiths shed detrital material into successions as old as latest Triassic basal Hazelton Group (Nelson et al., 2018; Hunter and van Straaten, 2020).

More regionally, the demise of the Quesnellia-Stikinia (Nicola-Stuhini) magmatic arcs in the Late Triassic is marked by arc uplift and local picritic magmatism, and followed by a period of prolific porphyry Cu emplacement in the latest Triassic to earliest Jurassic (Logan and Mihalynuk, 2014). Work in districts with young porphyry systems, where sea-floor bathymetry can be used to infer the architecture of subducting slabs, suggests that porphyry formation is commonly temporally associated with the subduction of aseismic ridges, seamount chains, and oceanic plateaus (Cooke et al., 2005). Furthermore, it has been suggested that subduction of such features may cause conditions favourable for porphyry emplacement through two primary mechanisms: 1) high-volume hydrous melt production within the mantle wedge followed by; 2) the development of local zones of extension that allow magmas to ascend (Richards et al., 2001; Richards, 2003; Cooke et al., 2005; Bertrand et al., 2014)

Logan and Mihalynuk (2014) proposed that subduction of an interarc complex, the Sitlika-Kutcho-Venables arc, resulted

**Table 1.** TIMS U-Pb zircon results and methods.

Sample (a)	Compositional Parameters										Radiogenic Isotope Ratios					Isotopic Ages							
	Wt. mg	U ppm	Pb ppm	Th U	$^{206}\text{Pb}^*/^{206}\text{Pb}^*$ $\times 10^{13}$ mol	mol % $^{206}\text{Pb}^*$	Pb* Pb <sub>c</sub>	Pb <sub>c</sub> (pg)	$^{206}\text{Pb}/^{204}\text{Pb}$	$^{208}\text{Pb}/^{206}\text{Pb}$	$^{207}\text{Pb}/^{206}\text{Pb}$	% err	$^{235}\text{U}/^{238}\text{U}$	$^{206}\text{Pb}/^{207}\text{Pb}$	corr. coef.	$^{207}\text{Pb}/^{206}\text{Pb}$	% err	$^{235}\text{U}/^{238}\text{U}$	$^{206}\text{Pb}/^{238}\text{U}$	$^{207}\text{Pb}/^{235}\text{U}$	$^{206}\text{Pb}/^{238}\text{U}$		
(a)	(b)	(c)	(c)	(d)	(e)	(c)	(e)	(f)	(g)	(g)	(g)	(h)	(g)	(i)	(h)	(i)	(h)	(i)	(h)	(i)	(h)	(i)	
2-1	0.0050	22	1.4	0.323	0.2878	98.65%	21	0.32	1371	0.102	0.05489	1.499	0.4835	1.617	0.06389	0.199	0.634	408	34	400.5	5.4	399.23	0.77
2-2	0.0023	108	9.3	0.918	0.7593	99.54%	73	0.29	4043	0.288	0.05611	0.232	0.5664	0.295	0.07321	0.105	0.708	456.7	5.2	455.7	1.1	455.47	0.46
2-7	0.0022	26	1.8	0.515	0.1552	98.02%	15	0.26	936	0.162	0.05485	1.216	0.4901	1.316	0.06481	0.169	0.630	406	27	405.0	4.4	404.81	0.66
2-8	0.0022	57	3.1	0.406	0.2657	98.65%	22	0.30	1375	0.128	0.05262	0.600	0.3652	0.662	0.05034	0.114	0.610	312	14	316.1	1.8	316.63	0.35
2-9	0.0017	258	9.9	0.955	0.5713	99.29%	48	0.34	2612	0.304	0.05006	0.381	0.2221	0.435	0.03218	0.097	0.629	197.6	8.9	203.64	0.80	204.16	0.20
T-3	0.0069	373	12.8	0.571	3.4628	99.89%	291	0.30	17434	0.181	0.05018	0.150	0.2232	0.221	0.03226	0.103	0.806	203.3	3.5	204.56	0.41	204.67	0.21
3-2	0.0006	360	13.3	0.358	0.3164	98.49%	19	0.40	1228	0.114	0.05050	0.678	0.2443	0.741	0.03509	0.111	0.619	218	16	221.9	1.5	222.31	0.24
3-7	0.0007	165	7.5	1.591	0.1547	97.86%	18	0.28	864	0.506	0.05033	2.130	0.2236	2.271	0.03222	0.184	0.789	210	49	204.9	4.2	204.43	0.37

(a) 1, 2 etc. are labels for fractions composed of single zircon grains or fragments; all fractions annealed and chemically abraded after Mattinson (2005) and Scoates and Friedman (2008).

(b) Nominal fraction weights estimated from photomicrographic grain dimensions, adjusted for partial dissolution during chemical abrasion.

(c) Nominal U and total Pb concentrations subject to uncertainty in photomicrographic estimation of weight and partial dissolution during chemical abrasion.

(d) Model Th/U ratio calculated from radiogenic  $^{208}\text{Pb}/^{206}\text{Pb}$  ratio and  $^{207}\text{Pb}/^{235}\text{U}$  age.

(e) Pb\* and Pb<sub>c</sub> represent radiogenic and common Pb, respectively; mol %  $^{206}\text{Pb}^*$  with respect to radiogenic, blank and initial common Pb.

(f) Measured ratio corrected for spike and fractionation only. Mass discrimination of  $0.25 \pm 0.04\%$  amu based on analysis of NBS-982; all Daly analyses.

(g) Corrected for fractionation, spike, and common Pb; all common Pb was assumed to be procedural blank:  $^{206}\text{Pb}/^{204}\text{Pb} = 18.50 \pm 1.0\%$ ;  $^{207}\text{Pb}/^{204}\text{Pb} = 15.50 \pm 1.0\%$ ;  $^{208}\text{Pb}/^{204}\text{Pb} = 38.40 \pm 1.0\%$  ( $\pm 1\sigma$ ).

(h) Errors are  $2\sigma$ , propagated using the algorithms of Schmitz and Schoene (2007) and Crowley et al. (2007).

(i) Calculations are based on the decay constants of Jaffey et al. (1971).  $^{206}\text{Pb}/^{238}\text{U}$  and  $^{207}\text{Pb}/^{235}\text{U}$  ages corrected for initial disequilibrium in  $^{230}\text{Th}/^{238}\text{U}$  using  $\text{Th}/\text{U}$  [magma] = 3.

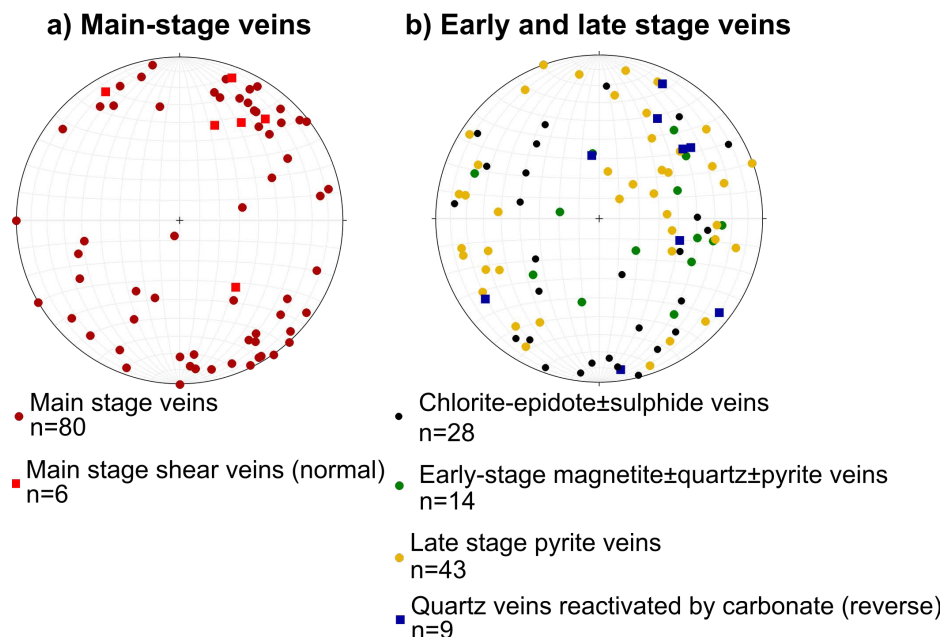


**Fig. 18.** Equal area stereonet showing poles to porphyry-related veins with interpreted relative timing. Note the contrast between the sheeted/orthogonal main-stage veins and the stockworked early and late-stage veins. **a)** Main-stage extensional quartz-chalcopyrite $\pm$ pyrite veins show two main orientations: NW-SE and E-S to NE-SW. Shear veins of identical mineralogy display down-dip motion. **b)** Early veins (magnetite-bearing), late-stage veins (massive sulphide) and veins with propylitic (epidote-chlorite-pyrite) assemblages of indeterminate timing have no discernible preferred orientation.

in buoyancy-driven stalling of subduction and arc-parallel tearing of the slab. The slab-tear associated with subduction of the Kutcho-Venables-Sitlika primitive arc resulted in the ingress of hot subslab mantle into the hydrated mantle wedge. Accordingly, this promoted extensive partial melting followed by lower degree partial melts that are associated with porphyry formation as the thermal perturbation decayed. Logan and Mihalynuk (2014) emphasised the role that orogen-parallel and transverse structures played in localizing porphyry deposits in Stikinia and Quesnellia.

Consistent with the perturbed subduction model proposed by Logan and Mihalynuk (2014), we suggest that oblique plate convergence during stalled subduction led to enhanced strain partitioning and inboard strike slip (e.g., Teyssier et al., 1995). Accordingly, local zones of extension related to this strike slip led to the formation of small pull-apart basins and permitted the ascent of magmas that formed Late Triassic porphyry deposits like the Big Bulk prospect.

## 9. Conclusions

Coarse conglomerates at the base of the Hazelton Group at Kinskuch Lake preserve evidence of syndepositional faulting and unroofing of the Stuhini Group in the latest Triassic. The prominent northeast-trending Tabletop fault bounds these conglomerates and defines the western edge of a high-relief depocenter in which conglomerates, including 120 m-scale megaclasts, accumulated. Systematic changes in clast size and composition within the conglomerates are related to syndepositional faults. We propose that in the latest Triassic,

the Tabletop fault was a northeast-trending strike-slip or oblique-slip fault and that subordinate east-west faults were generated in releasing step-overs or splays between it and other faults in the area. Syndepositional faulting is constrained to the Rhaetian (latest Triassic) from conodonts reported from a limestone megaclast in the conglomerates, a U-Pb zircon detrital maximum depositional age of  $206.7 \pm 1.9$  Ma from basal Hazelton (Hunter and van Straaten, 2020) and the cross-cutting relationships between the Big Bulk stock ( $204.61 \pm 0.18$  Ma, this paper) and the conglomerates. The east-west trend of the multiphase Big Bulk diorite stock, which hosts porphyry Cu-Au mineralization in sheeted quartz-chalcopyrite veins, is consistent with north-south extension during porphyry emplacement.

We suggest that latest Triassic to earliest Jurassic local basin formation in proximity (temporally and spatially) to porphyry systems is consistent with the stalled subduction model proposed by Logan and Mihalynuk (2014). Local extensional regimes and fault systems may have promoted and focussed the ascent of magmas associated with latest Triassic to early Jurassic porphyry Cu mineralization in northwestern British Columbia.

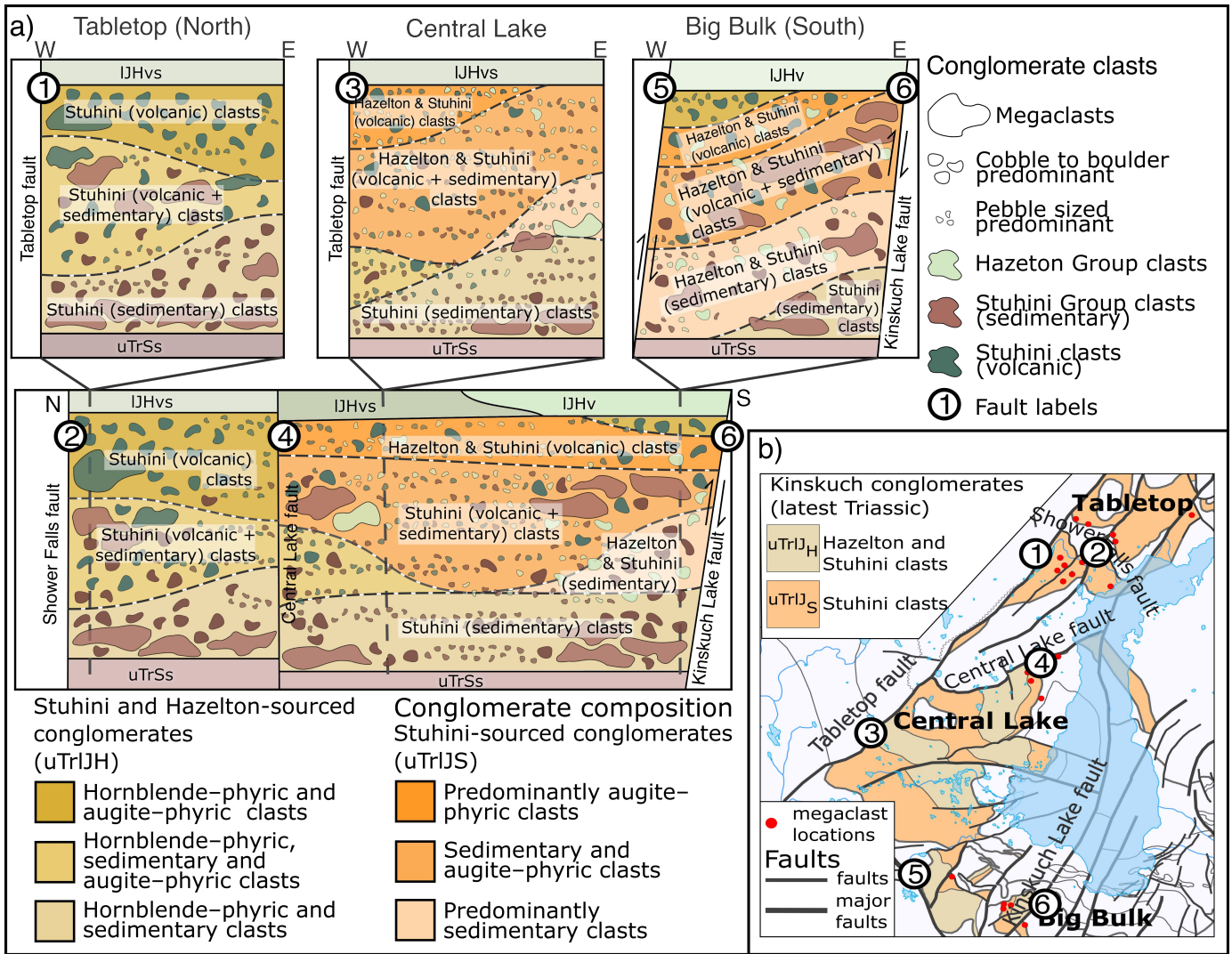


**Fig. 19.** Stratigraphic variation of clast compositions in the Kinskuch conglomerates. Contacts between conglomerates of different clast composition are presented as 6 main units to highlight the systematic vertical and lateral variation in clast content. **a)** At top, schematic stratigraphic section illustrating variations from east to west (relative to north-south trending faults); at bottom, schematic stratigraphic section illustrating variations from north to south (relative to east-west trending faults). **b)** Transitional conglomerate distribution in map view with locations and fault references for the stratigraphic sections presented in a).

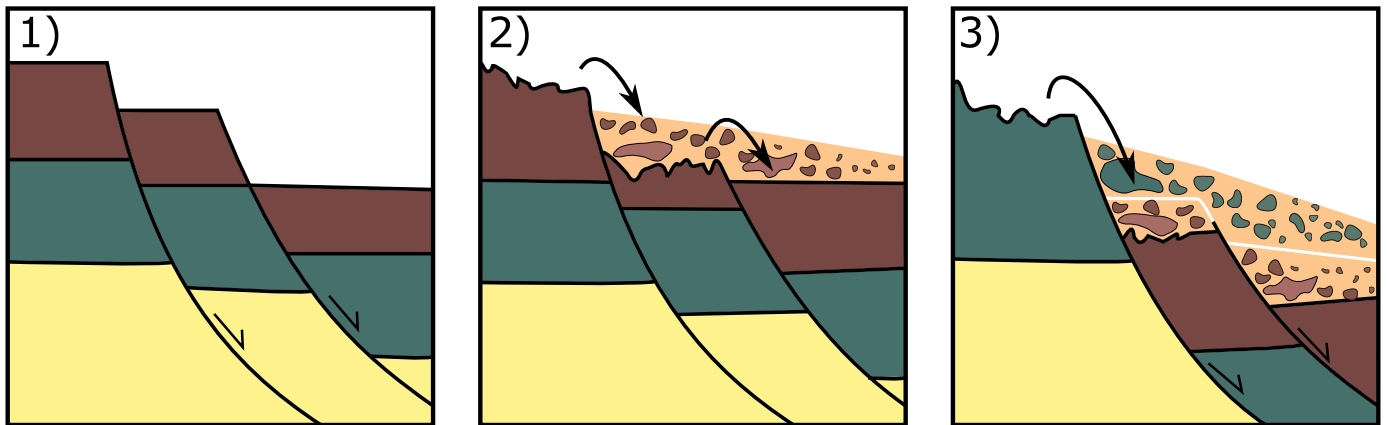


**Fig. 20.** Schematic diagram for generating the inverse stratigraphy recorded by clast compositions in the Kinskuch conglomerate by incision of the Stuhini Group to progressively deeper levels.

## Acknowledgments

Funding for this research was provided by a Natural Resources Canada-Targeted Geoscience Initiative Grant to Lori Kennedy and Bram van Straaten, a 2018 Geoscience BC scholarship to Emily Miller, and a Mitacs grant in conjunction with Dolly Varden and Norra Minerals. This project would not have been possible without the generous in-kind support provided by Dolly Varden Silver Corp., Norra Minerals, and Hecla Mining Company. Hayley McIntyre and Gayle Febbo generously provided their field descriptions, maps, and GIS data from work completed at Big Bulk during the 2017 field season. The authors deeply appreciate the very helpful reviews by Lawrence Aspler and JoAnne Nelson, which undoubtedly led to a significantly better manuscript.

## References cited

- Alldrick, D.J., 1993. Geology and metallogeny of the Stewart mining camp, British Columbia. British Columbia Ministry of Energy, Mines and Petroleum Resources Bulletin No. 85, 105 p.
- Alldrick, D.J., Dawson, G.L., Boshier, J.A., and Webster, I.C.L., 1986. Geology of the Kitsault river area (NTS 103P), British Columbia Ministry of Energy, Mines and Petroleum Resources, British Columbia Geological Survey, Open File 1986-02, 1:50,000 scale.
- Barresi, T., Nelson, J.L., Dostal, J., and Friedman, R., 2015. Evolution of the Hazelton arc near Terrace, British Columbia: stratigraphic, geochronological, and geochemical constraints on a Late Triassic - Early Jurassic arc and Cu-Au porphyry belt. *Canadian Journal of Earth Sciences*, 52, 466-494.
- Bertrand G., Guillou-Frottier, L., and Loiselet, C., 2014. Distribution of porphyry copper deposits along the western Tethyan and Andean subduction zones: Insights from a paleotectonic approach. *Ore Geology Reviews*, 60, 174-190.
- Brown, D.A., Gunning, M.H., and Greig, C.J., 1996. The Stikine project: Geology of western Telegraph Creek map area, northwestern British Columbia. British Columbia Ministry of Employment and Investment, British Columbia Geological Survey Bulletin 95, 175 p.
- Cloos, M., and Sapiie, B., 2013. Porphyry copper deposits: strike-slip faulting and throttling cupolas. *International Geology Review*, 55, 43-65.
- Cohen, K.M., Finney, S.C., Gibbard, P.L., and Fan, J.-X., 2013. The ICS international chronostratigraphic chart (updated, v. 2019/05), 36, 199-204.
- Colpron, M., and Nelson, J., 2011. A digital atlas of terranes for the northern Cordillera, BC. Ministry of Energy, Mines and Petroleum Resources, British Columbia Geological Survey, GeoFile 2011-11.
- Cooke D.R., Hollings, P., and Walshe, J.L., 2005. Giant porphyry deposits: Characteristics, distribution, and tectonic controls. *Economic Geology*, 100, 801-818.
- Cordey, F., Greig, C.J., and Orchard, M.J., 1992. Permian, Triassic, and Middle Jurassic microfaunal associations, Stikine terrane, Owegee and Kinskuch areas, northwestern British Columbia. In: *Current Research Part E*, Geological Survey of Canada Paper 92-1E, pp. 107-116.
- Edwards, B.R., and Russel, J.K., 2000. Distribution, nature, and origin of Neogene-Quaternary magmatism in the northern Cordilleran volcanic province, Canada. *Geological Survey of America Bulletin*, 112, 1280-1295.
- Evenchick, C.A., 2000. Northeast-trending folds in the western Skeena Fold Belt, northern Canadian Cordillera: a record of Early Cretaceous sinistral plate convergence. *Journal of Structural Geology*, 23, 1123-1140.
- Evenchick, C.A., McMechan, M.E., McNicoll, V.J., and Carr, S.D., 2007. A synthesis of the Jurassic-Cretaceous tectonic evolution of the central and southeastern Canadian Cordillera: exploring links across the orogen. In: Sears, J.W., Harms, T.A., Evenchick, C.A., (Eds.), *Whence the mountains? Inquiries into the evolution of orogenic systems: A volume in Honor of Raymond A. Price*. Geological Society of America Special Paper 433, pp. 117-145.
- Febbo, G.E., Kennedy, L.A., Nelson, J.L., Savell, M.J., Campbell, M.E., Creaser, R.A., Friedman, R.M., van Straaten, B.I., and Stein, H.J., 2019. The evolution and structural modification of the superergian Mitchell Au-Cu porphyry, northwestern British Columbia. *Economic Geology*, 114, 303-324.
- Gagnon, J.-F., Barresi, T., Waldron, J.W.F., Nelson, J.L., Poulton, T.P., Cordey, F., and Colpron, M., 2012. Stratigraphy of the upper Hazelton Group and the Jurassic evolution of the Stikine terrane, British Columbia. *Canadian Journal of Earth Sciences*, 49, 1027-1052.
- Golding, M.L., Orchard, M.J., and Zagorevski, A., 2017. Conodonts from the Stikine Terrane in northern British Columbia and southern Yukon. *Geological Survey of Canada Open File 8278*, 23 p.
- Gow, P.A., and Walshe, J.L., 2005. The role of pre-existing geologic architecture in the formation of giant porphyry-related Cu-Au deposits: Examples from New Guinea and Chile. *Economic Geology*, 100, 819-833.
- Greig, C.J., 1992. Fieldwork in the Owegee and Snowslide ranges and Kinskuch Lake area, northwestern British Columbia. In: *Current Research, Part A*, Geological Survey of Canada Paper 1992-1A, pp. 145-156.
- Greig, C.J., Cordey, F., and Orchard, M.J., 1995. Tectonic Significance of Early Permian to Late Triassic radiolarian cherts, Kinskuch Lake-Cambria Icefield area, SE of Stewart, NW BC; GAC/MAC annual meeting, Victoria '95, Program and abstracts, A38.
- Hunter, R.C., and van Straaten, B.I., 2020. Preliminary stratigraphy and geochronology of the Hazelton Group, Kitsault River area, Stikine terrane, northwest British Columbia. In: *Geological Fieldwork 2019*, British Columbia Ministry of Energy, Mines, and Petroleum Resources, British Columbia Geological Survey Paper 2020-1, pp. 101-118.
- Kyba, J., and Nelson, J., 2015. Stratigraphic and tectonic framework of the Khyber-Sericite-Pins mineralized trend, lower Iskut River, northwest British Columbia. In: *Geological Fieldwork 2014*, British Columbia Ministry of Energy, Mines and Petroleum Resources, British Columbia Geological Survey Paper 2015-1, pp. 41-58.
- Logan, J.M., and Koyanagi, V.M., 1994. Geology and mineral deposits of the Galore Creek area, northwestern British Columbia (104G/3 and 4). *British Columbia Ministry of Energy, Mines and Petroleum Resources, British Columbia Geological Survey Bulletin 92*, 96 p.
- Logan, J.M., and Mihalynuk, M.G., 2014. Tectonic controls on early Mesozoic paired alkaline porphyry deposit belts (Cu-Au±Ag-Pt-Pd-Mo) within the Canadian Cordillera. *Economic Geology*, 109, 827-858.
- Logan, J.M., Drobe, J.R., and McClelland, W.C., 2000. Geology of the Forest Kerr-Mess Creek area, northwestern British Columbia. *British Columbia Ministry of Energy, Mines and Petroleum Resources, British Columbia Geological Survey Bulletin 104*, 164 p.
- Nelson, J., and Kyba, J., 2014. Structural and stratigraphic control of porphyry and related mineralization in the Treaty Glacier-KSM-Brucejack-Stewart trend of western Stikinia. In: *Geological Fieldwork 2013*, BC Ministry of Energy, Mines and Petroleum Resources, BC Geological Survey Paper 2014-1, pp. 111-140.
- Nelson, J.L., Colpron, M., and Israel, S., 2013. The Cordillera of British Columbia, Yukon, and Alaska: Tectonics and Metallogeny.

- In: Colpron, M., Bissig, T., Rusk, B.G., Thompson, J.F.H., (Eds.), *Tectonics, Metallogeny, and Discovery: The North American Cordillera and Similar Accretionary Settings*. Society of Economic Geologists Special Publication 17, pp. 53-109.
- Nelson, J., Waldron, J., van Straaten, B., Zagorevski, A., and Rees, C., 2018. Revised stratigraphy of the Hazelton Group in the Iskut River region, northwestern British Columbia. In: *Geological Fieldwork 2017*, British Columbia Ministry of Energy, Mines and Petroleum Resources, British Columbia Geological Survey Paper 2018-01, pp. 15-38.
- Piquer, J., Skarmeta, J., and Cooke, D.R., 2015. Structural Evolution of the Rio Blanco-Los Bronces district, Andes of central Chile, controls on stratigraphy, magmatism and mineralization. *Economic Geology*, 110, 1195-2023.
- Richards, J.P., 2003. Tectono-magmatic precursors for porphyry Cu-(Mo-Au) deposit formation. *Economic Geology*, 98, 1515-1533.
- Richards, J.P., Boyce, A.J., and Pringle, M.S., 2001. Geological evolution of the Escondida area, Northern Chile: A model for spatial and temporal localization of porphyry Cu mineralization. *Economic Geology*, 96, 271-305.
- Sillitoe, R.H., 2010. Porphyry copper systems. *Economic Geology*, 105, 3-41.
- Teyssier, C., Tikoff, B., and Markley, M., 1995. Oblique plate motion and continental tectonics. *Geology*, 23, 447-450.
- Thorkelson, D.J., Mortensen, J.K., Marsden, H., and Taylor, D.C. 1995. Age and tectonic setting of Early Jurassic episodic volcanism along the northeastern margin of the Hazelton Trough, northern British Columbia. In: Miller, D.M., Busby, C.J., (Eds.), *Jurassic magmatism and tectonics of the North American Cordillera*. Geological Society of America Special Paper 299, pp. 83-94.
- Tombe, S.P., Richards, J.P., Greig, C.J., Board, W.S., Creaser, R.A., Muehlenbachs, K.A., Larson, P.B., DuFrane, S.A., and Spell, T., 2018. Origin of the high-grade Early Jurassic Brucejack epithermal Au-Ag deposits, Sulphurets mining camp, northwestern British Columbia. *Ore Geology Reviews*, 95, 480-517.
- Tosdal, R.M., Dilles, J.H., and Cooke, D.R., 2009. From source to sinks in auriferous magmatic-hydrothermal porphyry and epithermal deposits. *Elements*, 5, 289-295.
- van Straaten, B.I., and Nelson, J.L., 2016. Syncollisional late Early to early Late Jurassic volcanism, plutonism, and porphyry-style alteration on the northeastern margin of Stikinia. In: *Geological Fieldwork 2015*, British Columbia Ministry of Energy, Mines and Petroleum Resources, British Columbia Geological Survey Paper 2016-1, pp. 113-143.